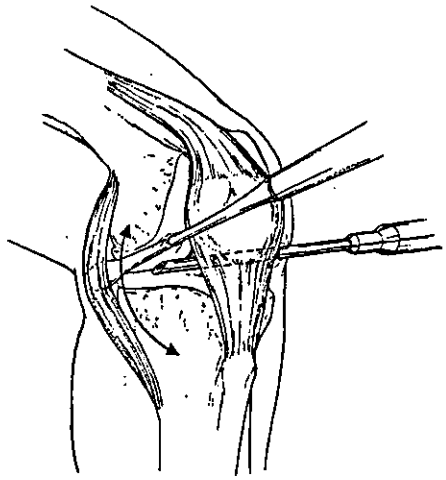

FIGURE 2. Arthroscopic PMR schematic: The medial side of the joint is released with a periosteal elevator under arthroscopy.

would conventionally be considered unsuitable for arthroscopic debridement. We first classified the knees based on magnetic resonance imaging (MRI) criteria and then analyzed the outcomes based on this classification.

METHODS

Fifty-eight medial-type OA knees in 52 patients with flexion contracture were treated with arthroscopic PMR in our hospital. A single surgeon performed all the procedures. Gender, age, radiographic grading using the Kellgren and Lawrence (K/L) system, range of motion (ROM), and the deviation of the axis on a standing radiograph were recorded at the time of the operation. All the patients had previously been treated conservatively, but because of their persisting knee pain, they had chosen to receive this additional treatment. Our procedure was applied to patients whose symptoms were restricted to the medial side of the knee joint. Patients with asymptomatic patellofemoral joint arthritic involvement were included in this series.

During PMR, we performed arthroscopic debridement, including meniscectomy of the degeneratively torn medial meniscus, excision of the unstable cartilage flap, and release of the joint capsule together with the MCL from the medial tibial plateau (Figs 1 and 2). Our meniscectomies were subtotal, i.e., the posterior two thirds of the medial meniscus was totally removed. Most intra-articular operations can be performed through the conventional two portals, i.e., the lateral and medial infra-patellar portals, but in our experience using midmedial or posteromedial portals made the meniscectomy of the posterior horn of the medial meniscus easier. Following the intra-articular procedure, valgus and extension stress were applied to the knee joint to further the release. Usually we heard a popping sound at this step. If we were unable to obtain enough joint space, i.e., if full extension and valgus instability at 30° of knee flexion were not obtained, we cut the tendon of the semimembranosus muscle. If this was not sufficient, we then cut the MCL transversely at the level of 1 cm below joint line. We did not do any further release if we could not achieve full extension after cutting those 2 structures. We injected hyaluronan intra-articularly once a week for 5 weeks postoperatively. Walking was encouraged from

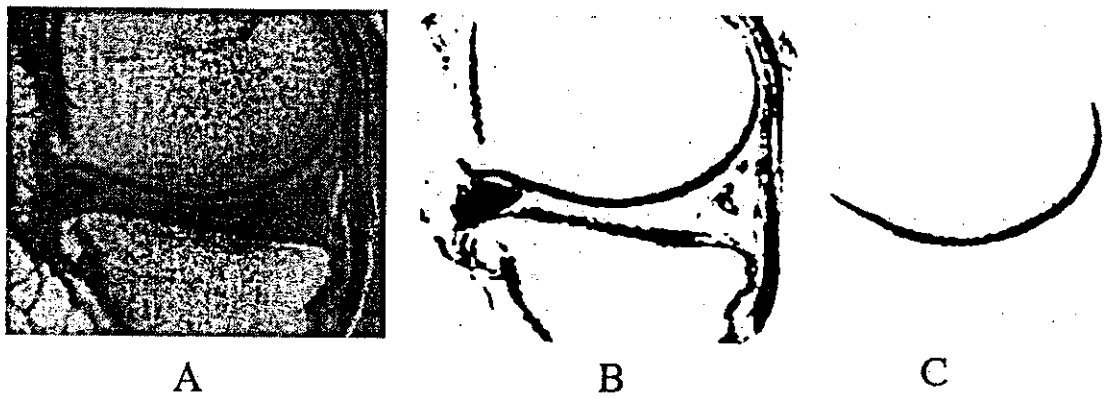

FIGURE 3. Extraction of the contour of the medial femoral condyle. (A) A proton-weighted sagittal image of the center of the medial compartment was scanned and (B) converted into a black and white image using image software. (C) The contour of the medial femoral condyle was extracted from this image and used for further assessment.

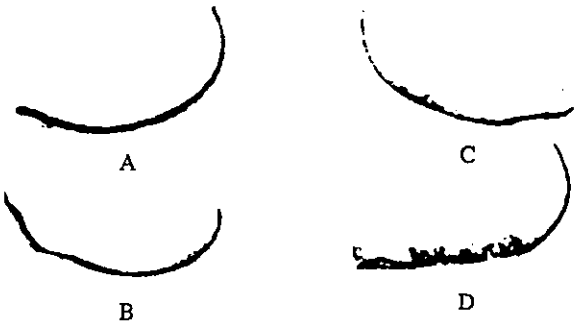

FIGURE 4. Classification of the contour of the medial femoral condyle. (A, B) Contour of the S group: Knees with medial femoral condyles with smooth contours or with minimum irregularity on MRI were classified as the S group. (C, D) Contour of the IR group: Knees with medial femoral condyles with irregular contours were classified as the IR group.

the day following surgery, as tolerated. Patients were evaluated at 3, 6, 12, 18, 24, 36, and 48 months after surgery. Clinical evaluation was performed using the Japanese Orthopaedic Association knee score (JOA score),[16,17] verbal rating score (VRS), and patient satisfaction, which were evaluated at the time of each follow-up. The JOA score is composed of 4 items: (1) pain on walking, (2) pain on ascending or descending stairs, (3) ROM, and (4) joint effusion. The VRS was used to estimate the severity of knee pain at the time of follow-up; patients were asked to rate their pain on a scale from 0 to 10, where the preoperative knee pain corresponded to 10. Patients rated their satisfaction as very satisfied, moderately satisfied, uncertain, or unsatisfied. The clinical outcomes of patients available for more than 2 years of follow-up are presented in this report. All of the evaluations were performed by a single orthopaedic knee surgeon who did not operate on any of the patients.

In addition to the overall analysis, we divided patients into 2 subgroups according to radiographic grade and preoperative MRI findings focusing on the regularity of the contour of the femoral condyle. The clinical outcome of each subgroup was compared using the JOA score. Only patients with knees rated grade III and IV in the K/L system were recruited. All MRI examinations were performed with a Signa 1.5-Tesla imager (GE Medical Systems, Milwaukee, WI), and proton-weighted images were used for evaluating the contour (FSE TR: 2000, TE: 12 msec, ETL: 4, time: 4 min 24 sec). To assess the regularity of the contour of the medial femoral condyle, we used computer image analysis. Sagittal MRIs of the medial femoral condyle were captured into a computer (PowerMac G3; Apple, Tokyo, Japan) using an image scanner (GT-7600; Epson, Tokyo, Japan), and converted into black and white images (Photoshop 5.0; Adobe, Tokyo, Japan). To determine the threshold between black and white, histograms of the intensity of the dots making the images were used. We determined the threshold so that only the structures with low signal intensity remained while those with isointensity to high intensity were deleted (Fig 3). After this manipulation, only the contour of the medial femoral condyle was extracted for evaluation. Patients whose medial femoral condyle was seen as smooth or with minimum irregularity on MRI were classified as the S group (Fig 4A and B), and those depicted with irregular contours on MRI were classified as the IR group (Fig 4C and D). Three knee surgeons independently classified the images as S or IR. If there was discrepancy, the decision was made by the majority.

A histologic examination was performed on specimens removed at the time of TKA. Pieces of bone cut out from the weight-bearing area of the medial femoral condyle were fixed with 10% (vol/vol) formaldehyde for 48 hours and decalcified with 20% EDTA for 10 days. The specimens were then processed and embedded in paraffin. Sections were cut at a thickness of 6 μm on a microtome and stained with H&E.

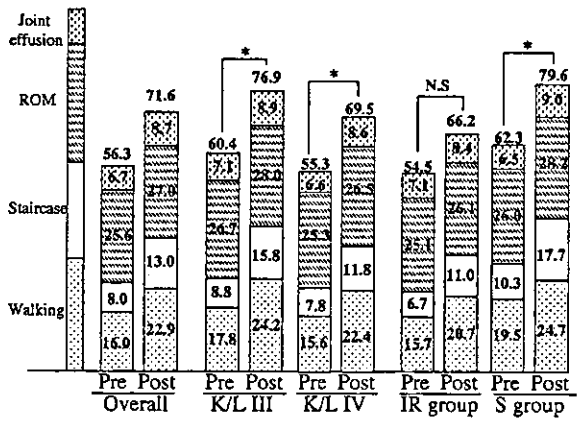

FIGURE 5. Comparison of the JOA scores before and after PMR. Average preoperative and postoperative JOA scores at the time of final follow-up are presented. The overall result is presented in the left 2 columns. Average preoperative and postoperataive JOA scores for subgroups that were classified with radiographic grading (grade III in the K/L grading and grade IV) as well as those divided by MRI findings (the IR group and the S group) are presented for comparison. Statistical analysis for comparing preoperative and postoperative JOA score was performed with the Wilcoxon signed-rank test. $P < .01$ was taken to be statistically significant. The P value for the IR group is more than 0.01 ($P = .011$), indicating a nonsignificant change. *, $P < .01$.

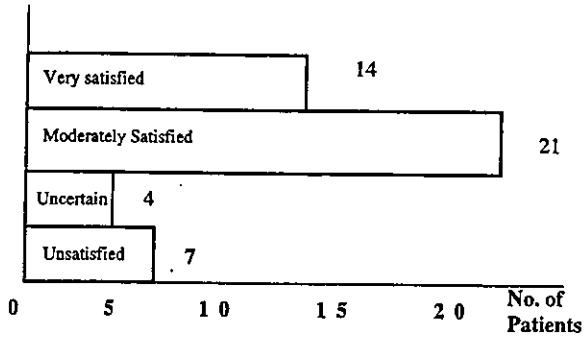

FIGURE 6. The patients' satisfaction at the time of final follow-up is presented. Their level of satisfaction was divided into 4 categories. The number of patients for each category is shown. Each patient who received a bilateral operation is counted as 1 patient on this measure.

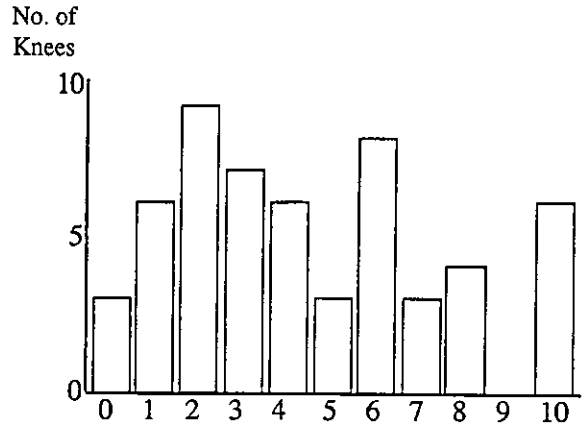

FIGURE 7. A VRS was used to assess the intensity of knee pain. The horizontal axis represents the intensity of the pain and the vertical axis represents the number of knees.

Statistical analysis for comparing preoperative and postoperative JOA score was performed using the Wilcoxon signed-rank test. $P < .01$ was considered to be statistically significant.

RESULTS

Fifty-eight medial-type OA knees in 52 patients (37 female and 15 male) with flexion contracture were treated with arthroscopic PMR in our hospital. The mean age of the patients at the time of surgery was 71.6 years (range, 47 to 84 years). The average ROM was from 13° to 129°. Six patients received bilateral surgeries; 2 were treated with simultaneous operations and 4 were treated with an interval of 10 to 16 months between operations. Seventeen knees were K/L grade III and 40 knees were grade IV. One case was classified as K/L grade II with flexion contracture of 10°.

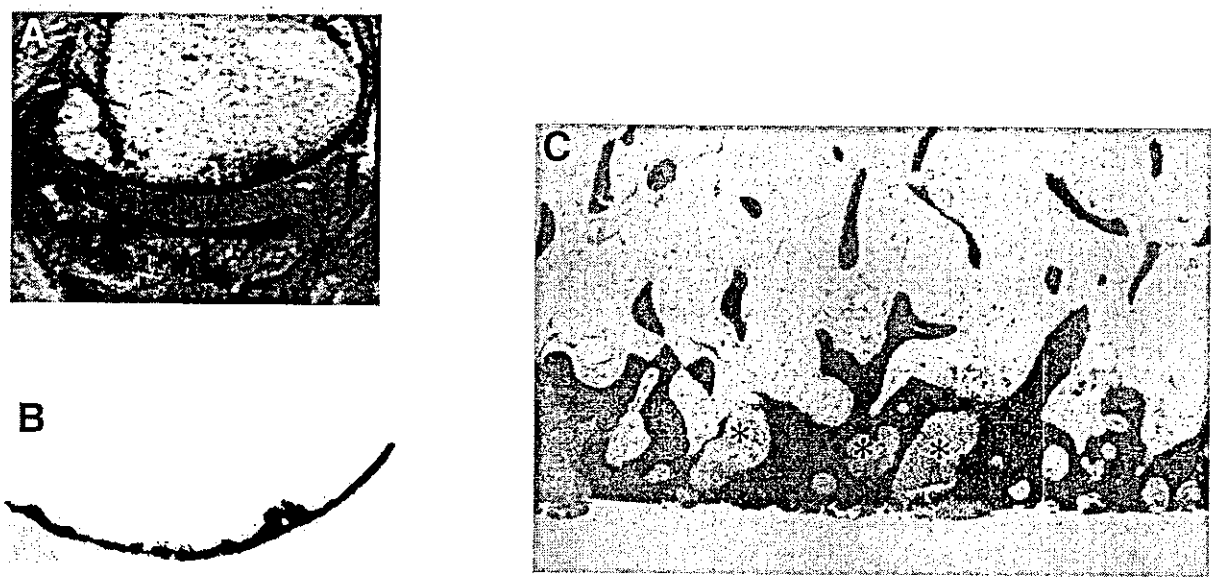

FIGURE 8. Histology of bones with irregular contours: (A) A sagittal MR image of the middle of the medial compartment of the knee joint. (B) Extraction of contour from image A revealed a medial femoral condyle, corresponding to the subchondral bone, with an irregular contour. (C) H&E staining revealed that the irregular contour was produced by the presence of multiple pseudo-cysts (*). Specimens were obtained at the time of TKA.

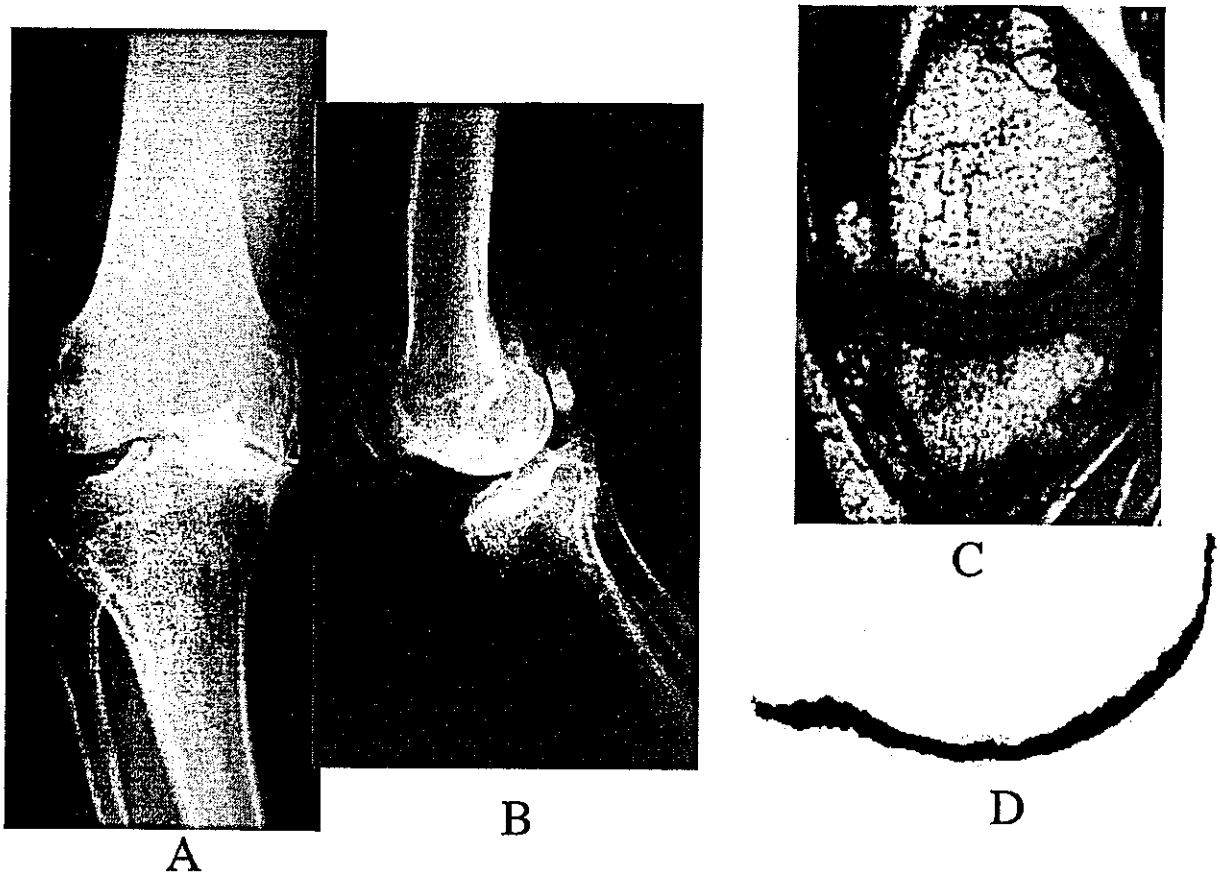

FIGURE 9. Case 1: A 76-year-old man with varus deformity of 7° was treated with arthroscopic PMR. (A) Standing anteroposterior radiograph showed a highly reduced joint space in his medial compartment. (B) Lateral radiograph showed slight arthritic changes in the patellofemoral (PF) joint. (C, D) MRI showed minimal irregularity in terms of the contour of the medial femoral condyle.

The patients had an average of 2.5° varus knee deformity.

Fifty-two knees belonging to 46 patients were available for more than 2 years of follow-up; the average follow-up period was 3.3 years (range, 2 to 4.8 years). Of these knees, 1 was K/L grade II, 16 were grade III, and 35 were grade IV.

Overall, the average JOA score improved from 56.3 points preoperatively to 71.6 points postoperatively (Fig 5). The average ROM at the time of last follow-up was from 6° to 130°. Seventy-six percent of patients (35 of 46 patients) were satisfied at their last follow-up (Fig 6). The VRS scores were reported as 0 to 2 for about one third of the knees (18 of 52 knees) and were not more than 5 for 65% of the knees (34 of 52 knees) (Fig 7). Although the knees exhibited valgus instability at 30° during follow-up examination, no patients were apprehensive that the knee would give way on walking.

The average JOA score for the K/L grade III knees improved to 76.9 from 60.4 points preoperatively, and that of the K/L grade IV knees improved to 69.5 from 55.3 points (Fig 5). The improvement in JOA scores was statistically significant for both groups.

Twenty-two knees were classified into the IR group based on MRI, and 24 knees were placed into the S group. MRI examinations of the other 6 knees were either not performed or not judged because of their poor image quality. The JOA score of the IR group improved to 66.2 points from 54.5 points preoperatively and that of the S group improved to 79.6 points from 62.3 points preoperatively (Fig 5). The postoperative JOA score was statistically higher only for the S group. Histologic examina-

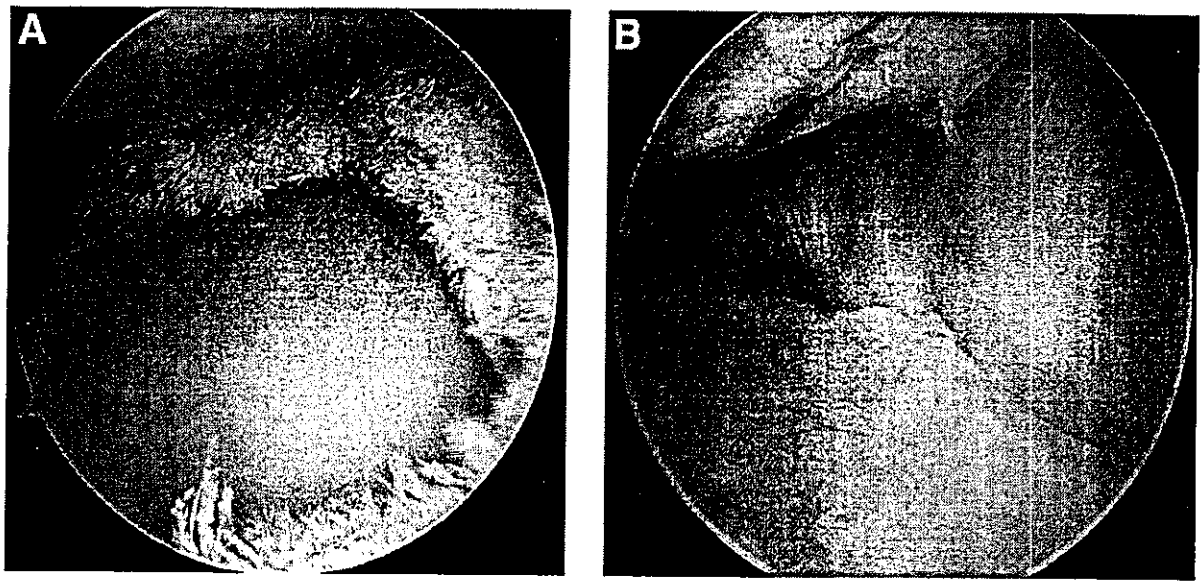

FIGURE 10. Second-look arthroscopy of case 1: (A) The preoperative state of the medial compartment. Extended eburnation of cartilage was observed on both femur and tibia. (B) Neither inflammatory synovium nor re-adhesion of released capsule was found in the medial compartment one year after PMR.

tion revealed that the irregularities of the femoral condyle seen on MRI were the result of microscopic multicystic changes of the subchondral bone (Fig 8).

A total of 6 knees were converted to TKA because of persistent knee pain. Five knees out of the 6 TKA cases belonged to the IR group and only 1 case belonged to the S group. The time from PMR to TKA ranged from 1.3 to 2.5 years.

Case 1

A 76-year-old man with varus deformity of 7° was treated with PMR. His radiograph was stage IV in the K/L system (Fig 9A). His JOA score was 55 preoperatively but improved to 80 points by 6 months after the PMR and was maintained at 80 points for 3 years postoperatively. His MRI showed minimal irregularity in terms of the contour of the medial femoral condyle (Fig 9B). This patient underwent arthroscopy just 1 year after PMR due to locking caused by the free body, which enabled us to see the state of the medial compartment at that time. Figure 10A shows the preoperative state of his medial compartment and Fig 10B shows the state 1 year after PMR. Extended eburnation of the joint surface was observed both on the femur and tibia before PMR (Fig 10A). Neither inflammatory synovitis nor re-adhesion of the released capsule was found in the medial compartment of his knee joint one year after PMR (Fig 10B).

Case 2

A 59-year-old woman with 1° of varus deformity was treated with PMR. A radiograph showed her knee was K/L grade III. Her MRI was classified as belonging to the IR group (Fig 11). Her JOA improved from 60 points preoperatively to 65 points 1.5 years postoperatively. The patient was not satisfied with the result.

DISCUSSION

In this report we present the clinical results of our arthroscopic PMR procedure as a surgical treatment option for medial-type OA knees. Overall, the JOA score improved 15 points, to an average score of 71.6 points following PMR. This is not as good as the results of TKA; in our hospital, 80 OA knees treated with TKA achieved an average score of 80.0 with an average follow-up of 2.5 years.[18] However, considering that all the knees in this series had flexion contracture and their radiographic grading showed advanced OA changes, this procedure is certainly of potential benefit for some patients because this arthroscopic operation is performed with the use of only 2 to 3 arthroscopic portals and does not lead to loss of

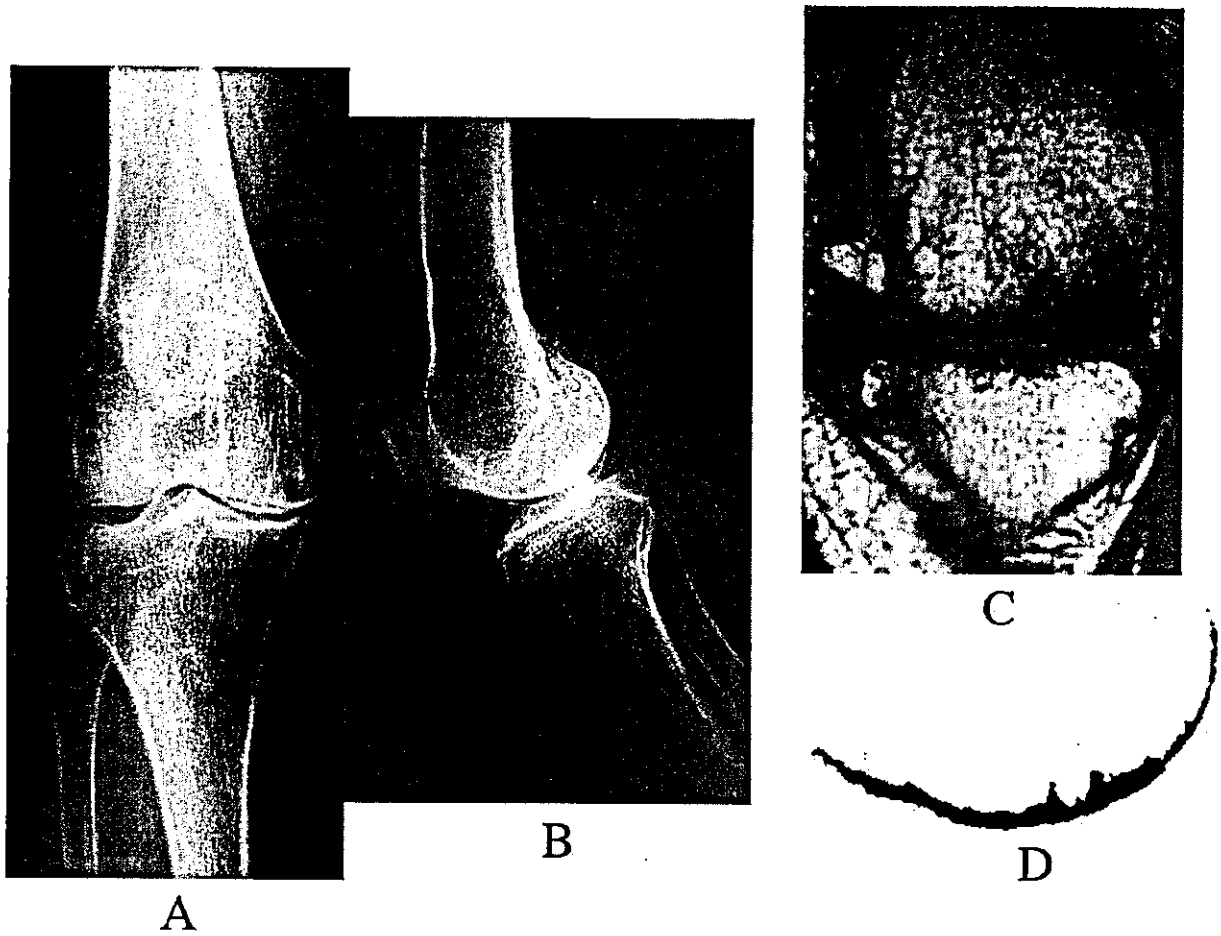

FIGURE 11. Case 2: A 59-year-old woman with 1° of varus deformity was treated with PMR. (A) Her radiograph indicated osteoarthritis of grade III in the K/L system. (B) Minimal arthritic change was observed in the patellofemoral joint. (C, D) Sagittal MRI of her medial compartment was used to classify her knee into the IR group.

ROM. The knees of the S group showed greater improvement, from 62.3 points preoperatively to 79.6 points postoperatively, a result equivalent to that of the TKA cases. We focused on the contour of the medial femoral condyle on MRI because our earlier study revealed that irregularity of the contour of the medial femoral condyle serves as an indicator of the clinical severity of medial-type OA.[19] In the present study, the patients' ages were somewhat different between the S and the IR group, although the radiographic grading of the 2 groups was almost identical (Table 1). Thus, the MRI findings are a significant factor in determining the clinical outcome of PMR. In contrast, grade IV knees obtained a statistically significant improvement in the JOA score, as did those of

TABLE 1. *Background of Patients*

	S Group	IR Group
Age (yr)	68.6 (47-82)	73.7 (58-90)
Lateral femorotibial angle	181.8° (177°-185°)	182.5° (177°-190°)
K/L Radiographic grade		
I	0	0
II	1	0
III	6	5
IV	12	13

NOTE. Basic information about the patients involved in the S or the IR classification is presented. Average age at the time of operation, varus deformity evaluated by standing anteroposterior radiograph, and distribution of Kellgren & Lawrence radiographic gradings are described.

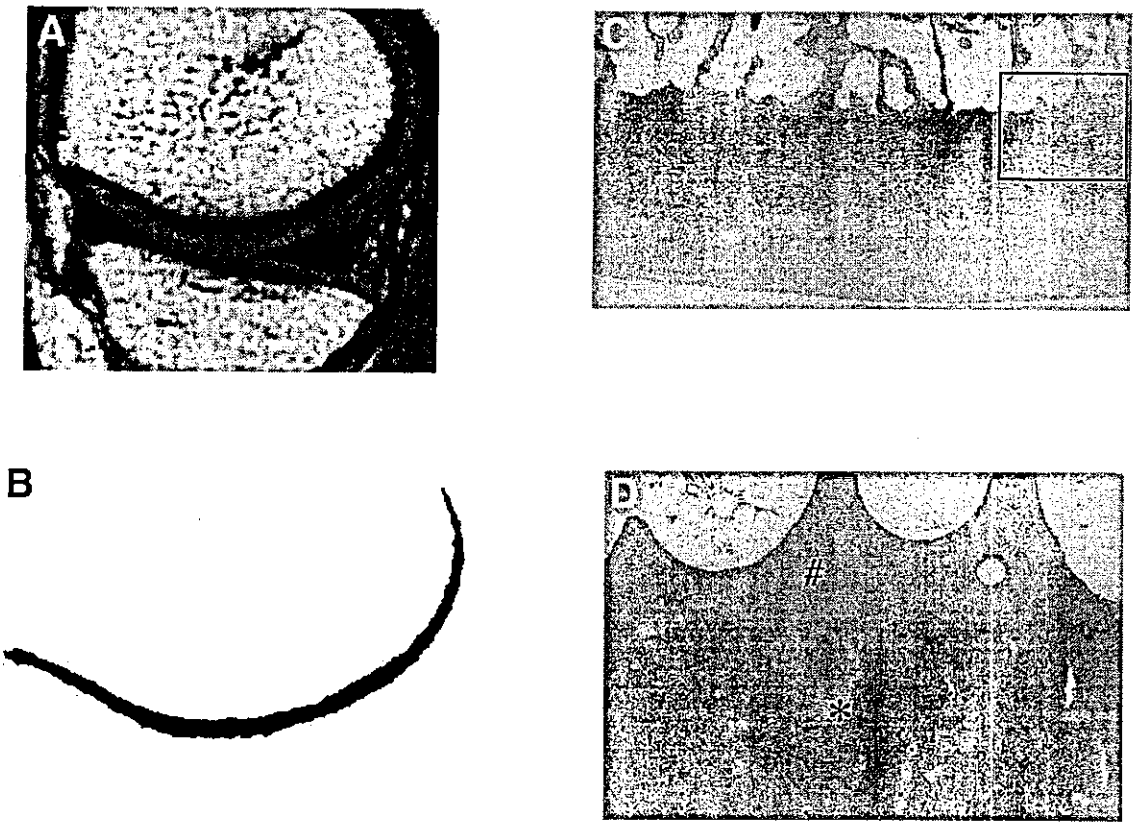

FIGURE 12. Histologic examination of a knee with a medial femoral condyle of smooth contour on MRI. (A) The original MRI and (B) an extracted contour. (C, low magnification; D, high magnification) Histologic examination of medial femoral condyle from this specimen shows the intact cartilage and regularly corrugated subchondral bone plate (#, subchondral bone; *, cartilage). The open box in C represents the area presented in D.

grade III, implying that radiographic grading does not decisively predict the outcome of PMR.

Based on pathologic examination, we concluded that the knees placed in the IR group contained advanced OA because the subchondral bone described on MRI as irregularly contoured was filled with multiple pseudocysts (Fig 8). In contrast, the smooth contours showed a regular subchondral pattern and no cysts (Fig 12; this specimen was obtained from a patient who suffered from a patellofemoral type OA knee and received TKA and who is not a case in this series). We conjecture that this pathologic change could lessen the effectiveness of bone-preserving procedures such as arthroscopic surgery or osteotomy. Several authors have reported benefits from arthroscopic debridement only when it was applied to knees in the early stages of OA.[6,7,8,20] In general, once OA knees have advanced beyond a certain stage, no arthroscopic treatment appears to be effective.

In 2001, Leon et al.[12] reported the clinical results of their ADMR procedure. Although they did not use any rating system for the assessment, they reported that their technique produced good results in 100% of their cases, and advocated the merit of releasing the medial side of the knee joint for medial-type arthritic knees. They stated that knees with more than grade III in the Ahlbach grading system are suitable for ADMR, which means that the OA of their patients was as severe as ours in terms of radiographic grading.[21] ADMR and PMR are different in the level of release and the approach to the medial meniscus. In ADMR, the release of the capsule is performed proximal to the medial meniscus but in PMR it is performed at the level of the tibial attachment. In ADMR, medial menisci are treated only when they are torn, but in PMR, medial menisci are excised in all cases; we observed that all of our cases had degeneratively torn menisci. ADMR and PMR are the same in terms of releasing

the medial side of the knee joint, but the clinical results of ADMR seemed to be better than our series. This may be simply due to the different techniques, but it is also possible to attribute this discrepancy to patient selection, the assessment method, or differences in lifestyle. However, the patient information that Leon et al. presented in their report was too restricted to allow comparison of these factors here.[12] We can state that we observed degeneratively torn menisci in all our cases without exception, which is consistent with the report by Jackson and Dieterichs[6] that degenerative menisci were seen in all of their patients with eburnated knees. On the other hand, some of the cases of Leon et al. had intact menisci, which may indicate that they treated some patients with earlier stages of OA in their series. We can also state that when TKA is required in the future, PMR gives the advantage of retaining the MCL as a ligamentous structure.

For postoperative care, we used hyaluronan once a week for 5 weeks with the expectation of inhibiting the released tissue from re-adhering to the medial tibial plateau. Hyaluronan is known to inhibit adhesive reactions from occurring in operatively damaged tissue.[22-24]

In conclusion, knees with relatively advanced medial-type OA with flexion contracture can potentially be successfully treated with PMR if their medial compartment is classified as S using MRI.

REFERENCES

1. Livesley PJ, Doherty M, Needoff M, Moulton A. Arthroscopic lavage of osteoarthritic knees. *J Bone Joint Surg Br* 1991;73: 922-926.
2. Hubbard MJS. Articular debridement versus washout for degeneration of the medial femoral condyle. *J Bone J Surg Br* 1996;78:217-219.
3. Shannon FJ, Devitt AT, Poyton AR, Fitzpatric P, Walsh MG. Short-term benefit of arthroscopic washout in degenerative arthritis of the knee. *Int Orthop* 2001;25:242-245.
4. McGinley BJ, Cushner FD, Scott WN. Debridement arthroscopy: 10-year follow-up. *Clin Orthop* 1999;367:190-194.
5. Richards RN Jr, Lonergan RP. Arthroscopic surgery for relief of pain in the osteoarthritic knee. *Orthopedics* 1984;7:1705-1707.
6. Jackson RW, Dieterichs C. The results of arthroscopic lavage and debridement of osteoarthritic knees based on the severity of degeneration: A 4- to 6-year symptomatic follow-up. *Arthroscopy* 2003;19:13-20.
7. Salisbuy RB, Nottage WM, Gardner V. The effects of alignment on results in arthroscopic debridement of the degenerative knee. *Clin Orthop* 1985;198:268-272.
8. Harwin SF. Arthroscopic debridement for osteoarthritis of the knee: Predictor of patient satisfaction. *Arthroscopy* 1999;15: 142-146.
9. Bert JM, Maschka K. The arthroscopic treatment of unicompartmental gonarthrosis: A five-year follow-up study of abrasion arthroplasty plus arthroscopic debridement and arthroscopic debridement alone. *Arthroscopy* 1989;5:25-32.
10. Rand JA. Role of arthroscopy in osteoarthritis of the knee. *Arthroscopy* 1991;7:358-363.
11. Moseley JB, O'Malley K, Petersen NJ, et al. A controlled trial of arthroscopic surgery for osteoarthritis of the knee. *N Engl J Med* 2002;347:81-88.
12. Leon HO, Blanco CER, Guithrie TB. Arthroscopic decompressive medial release of the varus arthritic knee: Expanding the functional envelope. *Arthroscopy* 2001;17:523-526.
13. Loeffler F. Die operative Behandlung der schweren schmerzhaften Arthrose des Kniegelenkes. *Zentralbl Chir* 1960;85: 1020-1023.
14. Schonbauer HR. Experience and results with the Loeffler operation for osteoarthritis of the knee joint. *Arch Orthop Unfallchir* 1976;85:337-346.
15. Reichel F, Muller-Stephann H. Loeffler's capsulotomy in advanced varus gonarthrosis. *Beitr Orthop Traumatol* 1988;35: 453-457.
16. The Japanese Orthopaedic Association Japanese Knee Society. *Assessment criteria for knee diseases and treatments*. Tokyo: Kanehara, 1994.
17. Wakabayashi S, Akizuki S, Takizawa T, Yasukawa Y. A comparison of the healing potential of fibrillated cartilage versus eburnated bone in osteoarthritic knees after high tibial osteotomy: An arthroscopic study with 1-year follow-up. *Arthroscopy* 2002;18:272-278.
18. Song L, Suzuki M, Tsuneizumi Y, Tsukeoka T, Moriya H. Clinical results of Hi-tech knee II total knee arthroplasty [in Japanese]. *Hiza* 2003;24:180-182.
19. Sasho T, Wada Y, Nakagawa K, Fujita K, Takahashi K, Moriya H. MRI as an indicator of disease progression and severity of osteoarthritis of the knee [in Japanese]. *Hiza* 2001; 22:222-225.
20. Fond J, Rodin D, Ahmad S, Nirschl RP. Arthroscopic debridement for the treatment of osteoarthritis of the knee: 2- and 5-year results. *Arthroscopy* 2002;18:829-834.
21. Petersson IF, Boegard T, Saxne T, Silman AJ, Svensson B. Radiographic osteoarthritis of the knee classified by the Ahlback and Kellgren & Lawrence systems for the tibiofemoral joint in people aged 35-54 years with chronic knee pain. *Ann Rheum Dis* 1997;56:493-496.
22. Abitbol JJ, Lincoln TL, Lind BI, Amiel D, Akeson WH, Garfin SR. Preventing postlaminectomy adhesion. A new experimental model. *Spine* 1994;19:1809-1814.
23. Burns JW, Skinner K, Colt J, et al. Prevention of tissue injury and post surgical adhesions by precoating tissues with hyaluronic acid solutions. *J Surg Res* 1995;59:644-652.
24. Moro-oka T, Miura H, Mawatari T, et al. Mixture of hyaluronic acid and phospholipid prevents adhesion formation on the injured flexor tendon in rabbits. *J Orthop Res* 2000;18: 835-840.

Research article

Distinct roles of Smad pathways and p38 pathways in cartilage-specific gene expression in synovial fibroblasts

Hiroaki Seto,[1,2] Satoshi Kamekura,[1] Toshiki Miura,[1] Aiichiro Yamamoto,[1] Hirotaka Chikuda,[1] Toru Ogata,[1] Hisatada Hiraoka,[1] Hiromi Oda,[1] Kozo Nakamura,[1] Hisashi Kurosawa,[2] Ung-il Chug,[3] Hiroshi Kawaguchi,[1] and Sakae Tanaka[1]

[1]Department of Orthopaedic Surgery, Faculty of Medicine, The University of Tokyo, Tokyo, Japan. [2]Department of Orthopaedics, Juntendo University School of Medicine, Tokyo, Japan. [3]Division of Tissue Engineering, University of Tokyo Hospital, Tokyo, Japan.

The role of TGF-β/bone morphogenetic protein signaling in the chondrogenic differentiation of human synovial fibroblasts (SFs) was examined with the adenovirus vector–mediated gene transduction system. Expression of constitutively active activin receptor–like kinase 3 ($ALK3^{CA}$) induced chondrocyte-specific gene expression in SFs cultured in pellets or in SF pellets transplanted into nude mice, in which both the Smad and p38 pathways are essential. To analyze downstream cascades of ALK3 signaling, we utilized adenovirus vectors carrying either Smad1 to stimulate Smad pathways or constitutively active MKK6 ($MKK6^{CA}$) to activate p38 pathways. Smad1 expression had a synergistic effect on $ALK3^{CA}$, while activation of p38 MAP kinase pathways alone by transduction of $MKK6^{CA}$ accelerated terminal chondrocytic differentiation, leading to type X collagen expression and enhanced mineralization. Overexpression of Smad1 prevented $MKK6^{CA}$-induced type X collagen expression and maintained type II collagen expression. In a mouse model of osteoarthritis, activated p38 expression as well as type X collagen staining was detected in osteochondrophytes and marginal synovial cells. These results suggest that SFs can be differentiated into chondrocytes via ALK3 activation and that stimulating Smad pathways and controlling p38 activation at the proper level can be a good therapeutic strategy for maintaining the healthy joint homeostasis and treating degenerative joint disorders.

Introduction

Injury to the articular cartilage occurs under various pathological conditions such as trauma, inflammation, and aging (1), and cartilage injury is followed by osteoarthritic changes of the affected joints. Osteoarthritis is the most common degenerative joint disorder, affecting nearly half of the elderly population. Osteoarthritis is characterized by degradation of articular cartilage and overgrowth of cartilage and bone, known as osteophytes, at the periphery of the articular surface, which results in pain and loss of joint function (1, 2). Microscopically, loss of proteoglycan and fibrillation of the articular surface are observed at the early stage of arthritis. At later stages, clefts are formed, and at the end stage, erosive changes in the articular cartilage appear. The high prevalence of this disease results in high costs for treating patients, and therefore the development of good therapeutics for osteoarthritis is a matter of great urgency. Because of the limited capacity of spontaneous healing, the regeneration of intact articular cartilage is one of the most challenging issues in the orthopedic field (3, 4). Transplantation of autologous chondrocytes or mesenchymal progenitor cells and autogenous osteochondral transplantation (mosaicplasty) have been successfully utilized for the repair of focal osteochondral defects (3, 5–11). However, the application of these technologies is limited to small defects due to the difficulty of obtaining a sufficient amount of cells or tissues.

Synovium is a thin tissue lining the nonarticular surfaces of diarthrodial joints (12). Synovial tissues contain various types of cells, including type A cells, macrophage lineage cells, and type B cells, which are specialized synovial fibroblasts (SFs). It is now widely recognized that synovial tissues are involved primarily in the pathogenesis of arthritic joint disorders such as rheumatoid arthritis by producing the matrix-degenerating enzymes cystein proteases and matrix metalloproteinases (MMPs) and the proinflammatory cytokines interleukin-1 (IL-1) and tumor necrosis factor-α (TNF-α) (12). We previously reported that SFs express a high level of receptor activator of NF-κB ligand, the osteoclast differentiation factor belonging to the TNF-α superfamily (13). In contrast to such catabolic actions, there is accumulating evidence that synovial cells have anabolic effects, leading to bone and cartilage production. Hunziker and Rosenburg reported that synovial cells can migrate into partial-thickness articular cartilage defects, where they proliferate and subsequently deposit a scar-like tissue (14). Nishimura et al. (15) demonstrated SFs show chondrogenic differentiation after being cultured in the presence of TGF-β, and de Bari et al. recently demonstrated that multipotent mesenchymal stem cells could be isolated from human synovial tissues, which differentiated into chondrocytes as well as osteoblasts, adipocytes, and myotubes under proper culture conditions (16, 17). Another dramatic clinical manifestation of the chondrogenic potential of synovial tissues is synovial chondromatosis, a tumor-like disorder characterized by the formation of multiple cartilaginous nodules, which is believed to be benign reactive metaplasia of synovial cells (18). These observations

Nonstandard abbreviations used: anterior cruciate ligament (ACL); bone morphogenetic protein (BMP); constitutively active activin receptor–like kinase 3 ($ALK3^{CA}$); constitutively active MKK6 ($MKK6^{CA}$); hemagglutinin (HA); matrix metalloproteinase (MMP); medial meniscus (MM); osteoarthritis (OA); receptor-regulated Smad (R-Smad); synovial fibroblast (SF); TGF-β–activating kinase 1 (TAK1).

Conflict of interest: The authors have declared that no conflict of interest exists.

Citation for this article: *J. Clin. Invest.* 113:718–726 (2004). doi:10.1172/JCI200419899.

lead us to speculate that synovial tissues contain multipotent cells with chondrogenic potential that might be involved in the repair process of articular cartilage defects and therefore might provide a good source for engineering articular cartilage.

There is accumulating evidence that TGF-β superfamily cytokines play an essential role in bone and cartilage development. Wozney and coworkers (19) reported that bone morphogenetic proteins (BMPs) induce early cartilage formation, and various studies have shown that TGF-β induces chondrocytic differentiation of undifferentiated mesenchymal cells (20–22). In the present study, we analyzed the role of TGF-β/BMP signaling on chondrogenic differentiation of human SFs by using the adenovirus vector–mediated gene transduction system. The introduction of an activated mutant of ALK3 (constitutively active activin receptor–like kinase 3 [ALK3^{CA}]), also known as BMP type IA receptor, induced chondrocyte-specific marker expression in the cells. ALK3 signaling involves two different downstream cascades, the Smad pathway and the p38 MAP kinase pathway. We used a combination of adenoviral gene delivery and chemical inhibition to analyze the role of these two signaling cascades in inducing differentiation of SF cells toward a chondrocyte phenotype and found that both pathways are essential for chondrogenic differentiation. Interestingly, activation of p38 pathways alone induced markers of terminal chondrocyte differentiation, type X collagen expression and mineralization, which was suppressed by Smad1 coexpression. These results suggest that both the Smad and p38 pathways are necessary for chondrogenic differentiation of SFs and that the balance between these two pathways determines the stage of differentiation.

Methods

Chemicals and antibodies. Alpha-modified minimum essential medium (α-MEM) was purchased from Gibco BRL, Life Technologies Inc. (Rockville, Maryland, USA), and fetal bovine serum (FBS), from Sigma-Aldrich (St. Louis, Missouri, USA). Anti-p38 MAPK and anti-phospho-p38 MAPK (Thr180/Tyr182) were obtained from Cell Signaling Inc. (Cummings Center, Beverly, Massachusetts, USA). Anti-Flag was purchased from Sigma-Aldrich, and anti-hemagglutinin (anti-HA) was from Santa Cruz Biotechnology Inc. (Santa Cruz, California, USA). Anti-phospho-Smad1/5/8, which recognizes the phosphorylated form of Smad1, Smad 5, and Smad8, and anti-phospho-Smad2 were from Cell Signaling Inc. Anti-type II collagen was purchased from Oncogen (Boston, Massachusetts, USA) and anti-type X collagen was from LSL Co. (Cosmo Bio, Tokyo, Japan). Other chemicals and reagents used in this study were of analytical grade.

Isolation of SFs from human synovial tissues. Synovial cells were obtained as previously described (13, 23, 24). In brief, with enzymatic digestion, human synovial cells were isolated from synovial tissues of the knee joints of ten rheumatoid arthritis patients (37–75 years of age; mean, 60.3 years of age) at the time of total knee arthroplasty operations. Written informed consent for subsequent experiments was obtained from each patient. Cells were suspended in α-MEM containing 10% FBS and were cultured in monolayers. After three to five passages, subcultured cells were composed of morphologically uniform fibroblastic cells (SFs) that were free of macrophages. They were infected with adenovirus vectors and cultured in pellets ("pellet culture"). Primary chondrocytes were obtained from articular cartilage resected during the surgeries. Cartilage was minced finely in phosphate-buffered saline (PBS), and chondrocytes were isolated by sequential digestion at 37°C with 0.25% (weight/volume) trypsin for 30 minutes and with 2 mg/ml of clostridial collagenase in α-MEM containing 10% FBS and antibiotics (penicillin at 100 μg/ml and streptomycin at 100 μg/ml) overnight on an orbital shaker. Cells were isolated by centrifugation and were resuspended in α-MEM with 10% FBS. Cells were cultured in monolayers for 1 day and then subjected to RNA isolation.

Constructs and gene transduction. The recombinant adenovirus vectors carrying various molecules that modulate TGF-β superfamily signaling pathways, that is, HA-tagged constitutively active TGF-β/BMP type I receptors (ALK3^{CA}, ALK5^{CA}, and ALK6^{CA}), constitutively active MKK6 (MKK6^{CA}), Flag-tagged Smad1 and Smad6 with CAG [cytomegalovirus IE enhancer + chicken β-actin promoter + rabbit β-globin poly(A) signal] promoter, were generated by the DNA-terminal protein complex method (25–27). SFs were infected with adenovirus vectors following a method previously described (13). In short, subconfluent SFs were incubated with a small amount of medium (α-MEM without serum) that contained the recombinant adenoviruses for 2 hours at 37°C at the indicated multiplicity of infection (MOI) and then with 10 times more medium to which 10% FBS had been added. Infected cells were cultured for additional 3 days for assessment of chondrogenic gene expression or were subjected to pellet culture 24 hours after the infection for histological examination.

Pellet cultures of isolated SFs. After 24 hours of viral infection, adherent cells were trypsinized and cells numbers were ascertained. Aliquots of 5×10^5 cells were spun down at 500 *g* in 15-ml polypropylene conical tubes in 5 ml of α-MEM with ascorbate 2-phosphate (0.1 mM) and 10% FBS. The cells were incubated at 37°C in 5% CO_2. Within 24 hours after incubation, the cells formed a single, free-floating pellet. The medium was changed every 2–3 days, and duplicate pellets were harvested after 3 and 7 days for real-time-PCR and Northern blotting and after 3 and 5 weeks for histological and immunohistochemical analysis. For visualization of the chondrogenic differentiation in vivo pellets were transplanted subcutaneously into *nu/nu* BALB mice (nude mice) after 3 days of pellet culture. Mice were sacrificed 5 weeks after transplantation and the pellets were recovered and subjected to toluidine blue staining as well as immunostaining with anti-type II collagen.

Immunoblotting. All the extraction procedures were performed at 4°C or on ice. Cells were washed with PBS and then lysed by the addition of TNE buffer (1% NP-40, 10 mM Tris-HCl, pH 7.8, 150 mM NaCl, 1 mM EDTA, 2 mM Na_3VO_4, 10 mM NaF, and 10 μg/ml aprotinin). Lysates were prepared by centrifugation at 10,000 *g* for 20 minutes. An equal amount (15 μg) of proteins was separated by electrophoresis on 10% SDS-polyacrylamide gels. After electrophoresis, proteins were electronically transferred onto a nitrocellulose membrane. Immunoblotting with specific antibodies was performed with ECL Western blotting reagents (Amersham Co., Arlington Heights, Illinois, USA) according to the conditions recommended by the supplier.

Histology and immunostaining. Pellet cultures were fixed with 3.7% formaldehyde, embedded in paraffin, and cut into sections 4 μm in thickness. Representative sections were subjected to Alcian blue staining, Alizarin red staining, and immunohistochemistry. Alcian blue staining was performed according to the protocol described previously (28). Briefly, after deparaffinization, sections were stained with 0.5% Alcian blue 8GX (Wako, Osaka, Japan) in 0.1 N HCl for 1 hour. Mineralization was assessed by Alizarin red staining. In brief, sections were immersed in Alizarin red solution (40 mM, at pH 4.0) for 8 minutes at room temperature, and nonspecific staining was removed by several washes in distilled water. For immunostaining with anti-type

II collagen or anti-type X collagen, we utilized a CSA Kit (DAKO, Carpinteria, California, USA) following the manufacturer's protocol.

Total RNA extraction and real-time PCR. Total RNA was isolated from SFs with ISOGEN (Wako) following the supplier's protocol. Complementary DNA (cDNA) was synthesized from 1 μg of total RNA with the Superscript II reverse transcriptase kit (Invitrogen, Carlsbad, California, USA). For real-time PCR, the ABI Prism Sequence Detection System 7000 was used. Primers were designed based on sequences obtained from GenBank and amplicons of 50–250 base pairs with a melting temperature of between 55°C and 60°C were selected. Aliquots of first-strand cDNA (1 μg) were amplified with the QuantiTect SYBER Green PCR Kit (Qiagen, Valencia, California, USA) under the following conditions: initial denaturation for 10 minutes at 94°C followed by 40 cycles consisting of 15 seconds at 94°C and 1 minute at 60°C. Data analysis consisted of fold induction, and the expression ratio was calculated from the differences in threshold cycles at which an increase in reporter fluorescence above a baseline signal could first be detected among three samples and was averaged for duplicate experiments. The primers we utilized in real-time PCR to detect sox9, type II collagen, type X collagen, osteocalcin, osteopontin, and GAPDH were as follows: sox9, 5′-AGAAGGACCACCCGGATTAC-3′ and 5′-AAGTCGATAGGGGGCTGTCT-3′; type II collagen, 5′-GGTGGCTTCCATTTCAGCTA-3′ and 5′-TACCGGTATGTTTCGTGCAG-3′; type X collagen, 5′-AGGAATGCCTGTGTCTGCTT-3′ and 5′-ACAGGCCTACCCAAACATGA-3′; osteocalcin, 5′-GTGCAGAGTCCAGCAAAGGT-3′ and 5′-CGATAGGCCTCCTGAAAGC-3′; osteopontin, 5′-ACAGCCAGGACTCCATTGAC-3′ and 5′-ACACTATCACCTCGGCCATC-3′; and GAPDH, 5′-GAAGGTGAAGGTCGGAGTCA-3′ and 5′-GAAGATGGTGATGGGATTTC-3′.

Northern blotting. Equal amounts (15 μg) of RNA were denatured in formaldehyde, separated by 1% agarose gel electrophoresis and transferred to a nitrocellulose membrane (Hybond N⁺) (Amersham Pharmacia, Piscataway, New Jersey, USA), followed by ultraviolet crosslinking. ULTRAHyb hybridization solution (Ambion, Austin, Texas, USA) was used according to the manufacturer's protocol. The blots were hybridized with a cDNA probe labeled with [α-^{32}P]dCTP using Ready-To-Go DNA Labeling Beads (Amersham Pharmacia). Rabbit type II collagen and aggrecan probes were generously provided by Yoshiyasu Iwamoto (Thomas Jefferson University, Philadelphia, Pennsylvania, USA). Membranes were washed in 2× SSC for 15 minutes at 42°C and then in 0.1× SSC for 30 minutes at 65°C. For visualization, X-ray film was exposed to membranes overnight at –80°C.

Osteoarthritis model mice. Osteoarthritic changes were developed in the knee joint by transection of the anterior cruciate ligament (ACL) and medial meniscus (MM) in C57BL/6 mice (mean age, 8 weeks) (29, 30). Briefly, after mice were anesthetized with ketamine and xylazine, a medial parapatellar skin incision was made. The subcutaneous tissues were incised and retracted, along with the articular capsule. The medial compartment of the knee joint was visualized and the ACL and MM were transected with a scalpel, and thereafter the capsule, medial retinaculum, and skin were sutured. Mice were housed in regular individual cages and allowed to exercise. Eight weeks after the surgery, the mice were sacrificed and paraffin-embedded sections of the affected joints were immunostained with anti-type X collagen and anti-phospho-p38 (Cell Signaling Technology Inc).

Results

Adenovirus-mediated gene transduction modulates the Smad and p38 pathways in SFs. We previously reported that adenovirus vectors can efficiently transduce foreign genes into synovial cells both in vitro and in vivo and that adenovirus infection itself does not affect the phenotypes of the cells (13). We constructed adenovirus vectors to analyze the role of ALK signaling as well as the Smad pathways and p38 pathways, which lie downstream of ALK signaling. SFs were infected with adenovirus vectors carrying various signaling molecules that modulate TGF-β superfamily signaling pathways, that is, HA-tagged constitutively active ALK3, ALK5, and ALK6 constitutively active MKK6, and Flag-tagged Smad1 and Smad6, as well as a control virus carrying the β-galactosidase gene (LacZ virus), and gene expression was determined by immunoblotting with specific antibodies. As shown in Figure 1, clear induction of the genes encoding ALK3^{CA}, ALK5^{CA} and ALK6^{CA} was observed by immunoblotting with anti-HA (Figure 1A), and Smad1 and 6, by anti-Flag (Figure 1B). ALK3^{CA} or ALK6^{CA} overexpression induced phosphorylation of Smad1, Smad5, and Smad8 in SFs, and ALK5^{CA}-transduced cells showed Smad2 phosphorylation (Figure 1A). MKK6^{CA} virus infection specifically activated p38 pathways in SFs, and the pathways were also activated in ALK3^{CA}-transduced cells as determined by Western blotting with anti-phospho-p38 (Figure 1C). The increased p38 phosphorylation induced by either ALK3^{CA} or MKK6^{CA} overexpression was suppressed by the p38-selective inhibitor SB203580.

Induction of chondrocyte-specific gene expression by ALK3^{CA} transduction in pellet cultures of SFs. To determine the effects of these transduced gene products on chondrocyte-specific gene expression in SFs, we subjected infected cells to pellet culture. After 7 days of culture, clear induction of type II collagen and aggrecan genes was observed in ALK3^{CA}-transduced cultures by both Northern blot analysis (Figure 2A) and real-time PCR (Figure 2, B and C). Expression of these genes was also observed in ALK6^{CA}-transduced cultures, albeit less efficiently, as shown in Figure 2, B and C, by real-time PCR. Contrary to the strong chondrogenic effects of ALK3^{CA} virus, expression

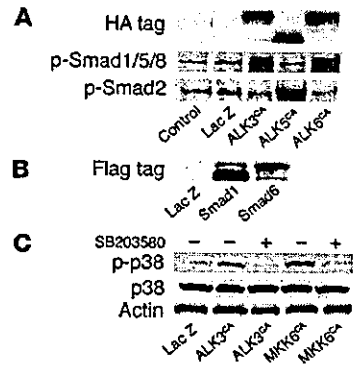

Figure 1
Modulation of intracellular signaling pathways by adenovirus vector–mediated gene transduction into SFs. (A) SFs at passage 3 were transduced with HA-tagged constitutively active ALK3, ALK5, and ALK6, and the expressed products were detected by immunoblotting after 2 days of viral infection. Expression of these genes was detected by immunoblotting with anti-HA and phospho-Smad1, -Smad 5, and Smad8 (p-Smad1/5/8) was observed in cells expressing ALK3^{CA} or ALK6^{CA}, and p-Smad2, in cells expressing ALK5^{CA}. (B) Expression of Smad1 and 6 in SFs was determined by anti-Flag. (C) Adenovirus vector–mediated ALK^{CA} or MKK6^{CA} expression specifically activated p38 pathways in SFs, as determined by Western blotting with anti-phospho-p38 (p-p38). The increased p38 phosphorylation induced by ALK3^{CA} or MKK6^{CA} overexpression was suppressed by the p38-selective inhibitor SB203580.

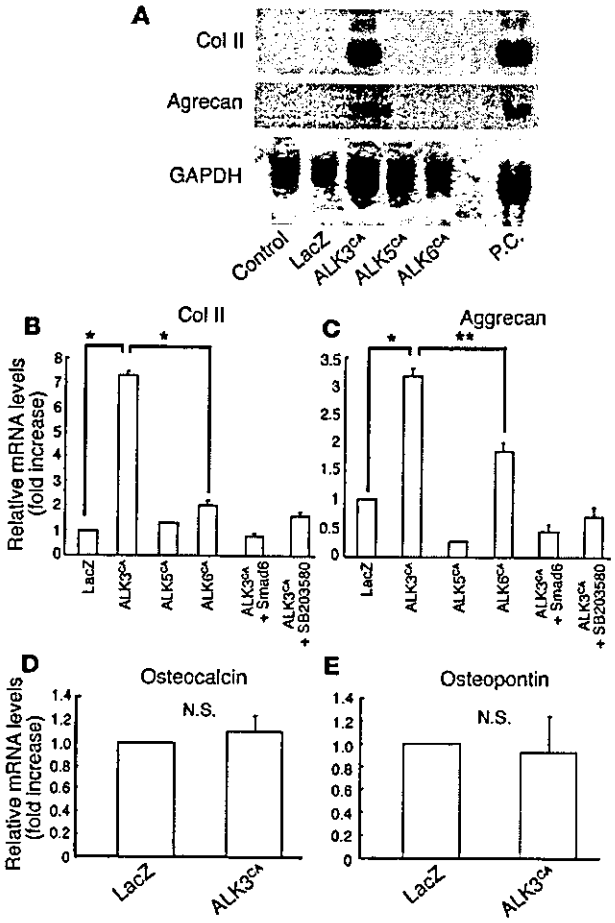

Figure 2
Effects of ALK3^{CA}, ALK5^{CA}, and ALK6^{CA} expression on chondrocyte-specific gene expression in SFs. (A–E) Gene expression in SFs, as determined by Northern blot analysis (A) and real-time PCR analysis (B–E). Subconfluent monolayer SF cultures were infected with adenovirus vectors and they were then subjected to pellet culture 24 hours after viral infection; mRNA extracted from the pellets after 7 days of culture was then analyzed. Expression of type II collagen (Col II) and aggrecan was clearly induced in ALK3^{CA}-expressing cultures, as shown by Northern blot analysis (A) and real-time PCR analysis (B and C); this was suppressed by Smad6 coexpression and SB203580 (B and C). Expression of type II collagen and aggrecan was also observed in ALK6^{CA}-expressing cultures, albeit less efficiently, as shown in B and C by real-time PCR. Neither the osteocalcin nor the osteopontin gene was induced by ALK3^{CA} virus infection (D and E). P.C., positive control, which represents the Northern blotting using mRNA of primary chondrocytes. N.S., not significant; $^{*}P < 0.001$; $^{**}P < 0.005$ (significantly different).

of osteocalcin or osteopontin was hardly detectable in the cells (Figure 2, C and D), indicating that hypertrophic and osteogenic differentiation were somehow blocked in these cultures. In contrast, neither type II collagen nor aggrecan gene expression was observed in ALK5^{CA} virus-infected cells (Figure 2, A–C). Type II collagen and aggrecan expression induced by ALK3^{CA} transduction was completely suppressed by coexpression with Smad6 or by SB203580 (Figure 2, B and C).

ALK3 gene transduction increases Alcian blue–positive matrix and type II collagen deposition in pellet cultures of SFs. For histological analysis, cells were subjected to pellet culture 24 hours after the viral infection. After 3 weeks of pellet culture, cells were fixed and examined by Alcian blue staining (Figure 3, A, D, G, and I) and Alizarin red staining and type II collagen immunostaining (Figure 3, B, E, G, and J) and type X collagen immunostaining (Figure 3, C and F). ALK3^{CA} virus-infected cultures showed cartilageous matrix production that was strongly positive for Alcian blue staining (Figure 3D), while no positive staining was observed in LacZ virus-infected cultures (Figure 3A) or ALK5^{CA} virus-infected cultures (Figure 3G), and only weak staining was observed in ALK6^{CA} virus-infected cultures (Figure 3H). No Alizarin red staining was observed in ALK3^{CA}-infected cultures (not shown), indicating that mineralization associated with osteogenic differentiation was not induced. ALK3^{CA} virus-infected SFs showed an oval shape, morphologically reminiscent of chondrocytes (Figure 3D). Immunostaining with anti-type II collagen showed positive staining in ALK3^{CA} virus-infected pellet cultures (Figure 3E) and weak staining in ALK6^{CA} virus-infected cultures (Figure 3H), while we failed to detect type X collagen in ALK3^{CA} virus-infected cultures (Figure 3F), which suggests an absence of terminal differentiation to hypertrophic chondrocytes. No positive type II collagen immunostaining was detected in LacZ virus-infected cultures (Figure 3B) or ALK5^{CA} virus-infected cultures (Figure 3H).

ALK3^{CA}-transduced SFs after pellet culture form cartilage matrix in vivo. To study chondrogenic differentiation of SFs in vivo, we subcutaneously transplanted the pellets into nude mice. Mice were sacrificed 3 weeks after the transplantation and the pellets were recovered and subjected to histological analysis. The transplanted SF pellets expressing ALK3^{CA} were positively stained for toluidine blue (Figure 4C), which detects proteoglycan components, as does Alcian blue staining. Type II collagen immunostaining was also positive (Figure 4D), indicating the cartilaginous differentiation of the cultures in vivo, while Alizarin red staining was almost undetectable (data not shown). ALK6^{CA} expression also induced chondrogenesis, albeit much less prominently (not shown), while neither LacZ (Figure 4, A and B) or ALK5^{CA} (not shown) expression could induce chondrogenic phenotypes in the cultures. The histological observation was further confirmed by real-time PCR; expression of type II collagen and aggrecan was significantly higher in ALK3^{CA}-transduced pellets (Figure 4, E and F). These results suggest that ALK3^{CA}

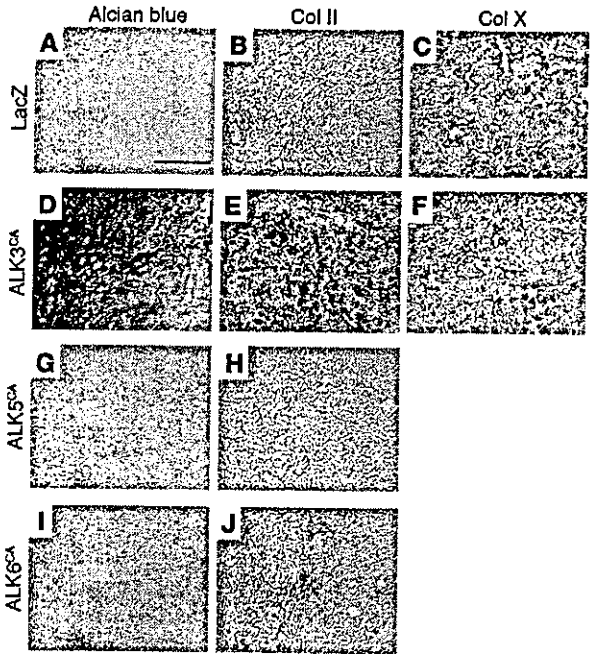

Figure 3
ALK3^{CA} gene transduction increases Alcian blue–positive matrix and type II collagen deposition in pellet cultures of SFs. (**A**–**J**) Adenovirus–infected SF pellets were fixed with 3.7% formaldehyde after 3 weeks of culture and then were subjected to Alcian blue staining (**A**, **D**, **G**, and **I**) or immunostaining with anti–type II collagen (**B**, **E**, **H**, and **J**) or anti–type X collagen (Col X) (**C** and **F**). Distinct Alcian blue (**D**) and type II collagen (**E**) staining was observed in ALK3^{CA}-expressing cultures. ALK6^{CA}-expressing cultures showed weaker staining (**I** and **J**), and no positive staining was observed in ALK5^{CA} virus–infected (**G** and **H**) or LacZ virus–infected (**A** and **B**) cultures. No type X collagen immunostaining was observed in cultures expressing LacZ or ALK3^{CA} (**C** and **F**). Scale bar: 100 μm.

overexpression was able to target cartilage formation without subsequent bone formation in vivo.

Segregation of ALK signaling pathways. ALK signaling is known to be mediated by both the Smad pathways and MAP kinase pathways, especially the p38 pathways (31–33). We therefore attempted to distinguish the roles of the Smad pathways and p38 pathways from each other using a specific p38 inhibitor or adenovirus vectors. Smad6 coexpression or treatment of the cultures with the p38 inhibitor SB203580 completely abrogated the chondrogenic gene expression induced by ALK3^{CA} (Figure 2, B and C). These results indicate that both the Smad pathways and the p38 MAP kinase pathways are required for the differentiation. Although Smad1 expression alone (MOI = 20) or a small amount of ALK^{CA} virus (MOI = 2) failed to induce type II collagen expression in SFs, both had synergistic effects, and robust upregulation of type II collagen gene was observed by coinfection of Smad1 virus (MOI = 20) and ALK3^{CA} virus (MOI = 2) (Figure 5A). Interestingly, activation of p38 pathways alone by MKK6^{CA} expression in SFs induced rapid induction of Sox9 and type II collagen, which declined rapidly, however, and type X collagen expression was subsequently increased (Figure 5B). Coexpression of Smad1 together with MKK6^{CA} not only reduced type X collagen expression but also maintained type II collagen expression in the cells (Figure 5B). Pellet cultures infected

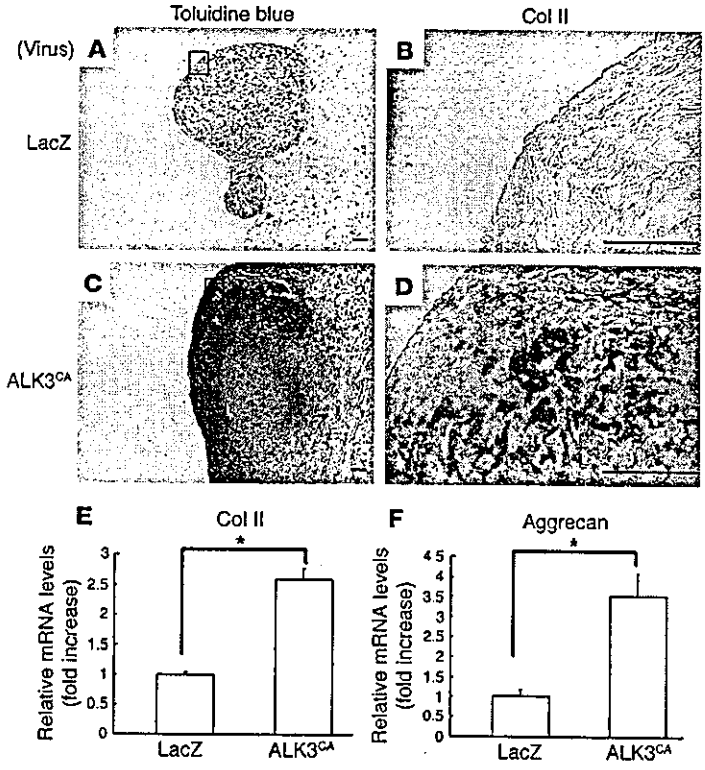

Figure 4
ALK3^{CA}-transduced SFs form cartilage matrix in vivo. (**A**–**D**) Three weeks after transplantation into nude mice, pellets were recovered and stained with toluidine blue (**A** and **C**) and immunostained with anti–type II collagen (**B** and **D**). Type II collagen immunohistochemistry was shown in the enlarged features of the rectangular area in the toluidine blue staining. Distinct positive staining was observed in ALK3^{CA}-expressing cultures (**B** and **D**) in contrast to LacZ virus–infected cultures (**A** and **C**). Scale bars: 100 μm. (**E** and **F**) Real-time PCR analysis of type II collagen and aggrecan. Their expression was significantly higher in ALK3^{CA}-expressing pellets than in LacZ-expressing pellets. *$P < 0.001$ (significantly different).

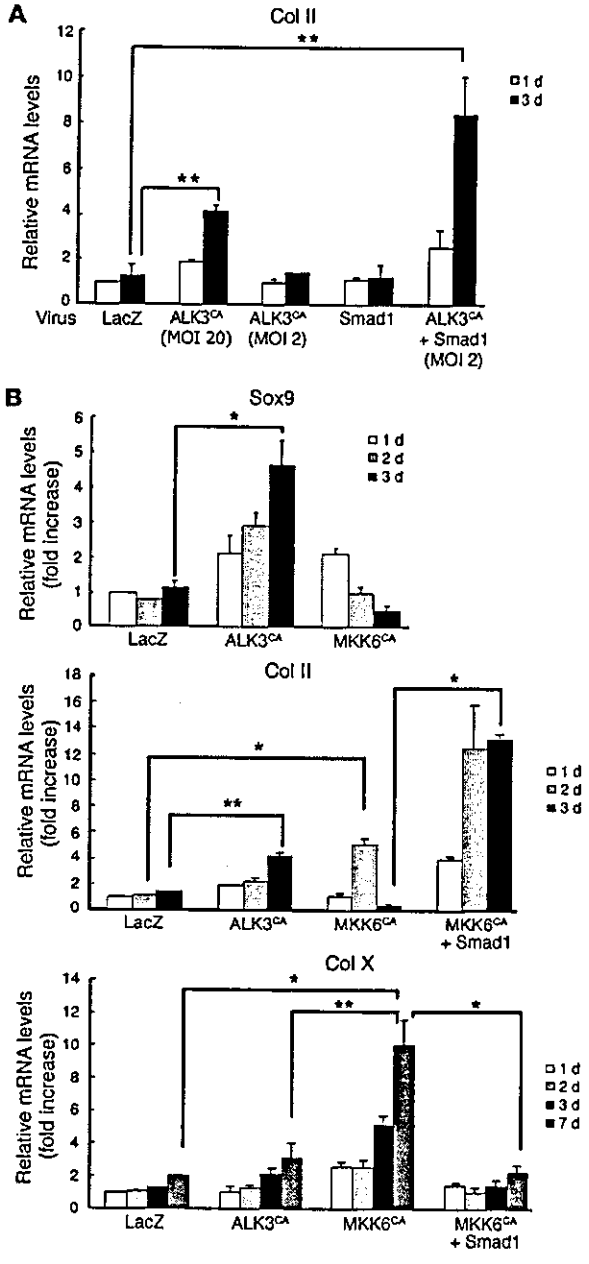

Figure 5
Segregation of downstream signaling pathways of ALK3. (**A**) Synergistic effect of Smad1 expression on the chondrogenic effects of the $ALK3^{CA}$ virus. Expression of Smad1 (MOI = 20) together with $ALK3^{CA}$ virus (MOI = 2) strongly induced expression of type II collagen in SFs. White bars indicate type II collagen expression on day 1 of cultures, and black bars indicate that on day 3. $^{**}P < 0.005$ (significantly different). (**B**) MKK6-p38 pathways promote terminal chondrocytic differentiation of SFs. Mandatory activation of p38 pathways by expression of $MKK6^{CA}$ using adenovirus vectors rapidly activated expression of the Sox9 and type II collagen genes, which rapidly declined, while expression of a terminal chondrocytic differentiation marker, type X collagen, was gradually increased. Adenovirus vector–mediated overexpression of Smad1 together with $MKK6^{CA}$ suppressed type X collagen expression and maintained type II collagen expression in SFs. $^{*}P < 0.001$; $^{**}P < 0.005$ (significantly different).

with $MKK6^{CA}$ virus were positively stained by type X collagen immunostaining as well as Alizarin red staining, which was suppressed by Smad1 virus coinfection (Figure 6).

Type X collagen expression and p38 activation in synovial cells in osteoarthritic joints. To examine the role of p38 activation in the development of degenerative changes in the articular cartilage, we next analyzed synovial tissues in the mouse model of osteoarthritis. After ACL and MM resection, the animals developed degenerative joint changes mimicking osteoarthritis. Osteochondrophytes were formed at the posterior edge of the femoral condyle and they were positively stained by anti-type X collagen as well as toluidine blue (rectangular areas in Figure 7, A and C) 4 weeks after the operation (corresponding to the stage of moderate osteoarthritis). Clusters of migrating synovial cells were observed adjacent to the osteochondrophytes (Figure 7B, arrowheads), where future osteochondrophytes will develop, and they were weakly stained by toluidine blue and anti-type X collagen at the marginal area between synovium and osteophytes (rectangular areas in Figure 7, B and D). This region was also positively stained by anti-phospho-p38 (Figure 7F). No positive staining was observed in the normal synovium, however (data not shown).

Discussion

The signaling events leading to chondrogenesis still remain elusive, although there is accumulating evidence that TGF-β superfamily cytokines may play an important role (19–22). The receptors of TGF-β family members are composed of two different types of serine/threonine kinase receptors, known as type I and type II (31, 34, 35). Type II receptors are constitutively active kinases and phosphorylate type I receptors, also called ALKs. Type I receptors in turn mediate specific intracellular signaling pathways and therefore determine the specificity of the downstream signaling. So far, seven type I receptors have been identified, ALKs 1–7. ALK3 (BMPR-IA) and ALK6 (BMPR-IB) are structurally similar to each other and function as BMP receptors, while ALK5 and ALK4 work as type I TGF-β receptors. Using the adenovirus vector system, Fujii et al. reported that $ALK1^{CA}$, $ALK2^{CA}$, $ALK3^{CA}$, and $ALK6^{CA}$ induced osteoblastic differentiation of C2C12 myoblasts and that $ALK3^{CA}$ or $ALK6^{CA}$ introduction induced chondrocytic differentiation of ATDC teratocarcinoma cells (27).

In the present study, we focused on the regulation of chondrogenic differentiation of primary SFs obtained from rheumatoid arthritis patients. SFs have chondrogenic potential (15, 16) and can migrate into articular cartilage defects, where they deposit a scar-like tissue as Hunziker et al. pointed out (14), suggesting that SFs have anabolic effects on joint homeostasis and are involved in the restoration process of articular cartilage. We demonstrated that adenovirus vector–mediated $ALK3^{CA}$ gene expression induced robust induction of chondrocyte-specific gene expression in SFs in a ligand-independent manner. Clear induction of Sox9, a key transcription factor regulating chondrogenesis (36, 37), followed by type II collagen and aggrecan expression, was observed in the $ALK3^{CA}$-expressing cultures, while type X collagen was only weakly induced in the cultures and no osteocalcin expression could be found (Figures 2 and 5). Induction of these chondrocyte-specific genes through $ALK3^{CA}$ expression was not observed in skin fibroblasts, suggesting the cell specificity of the events (data not

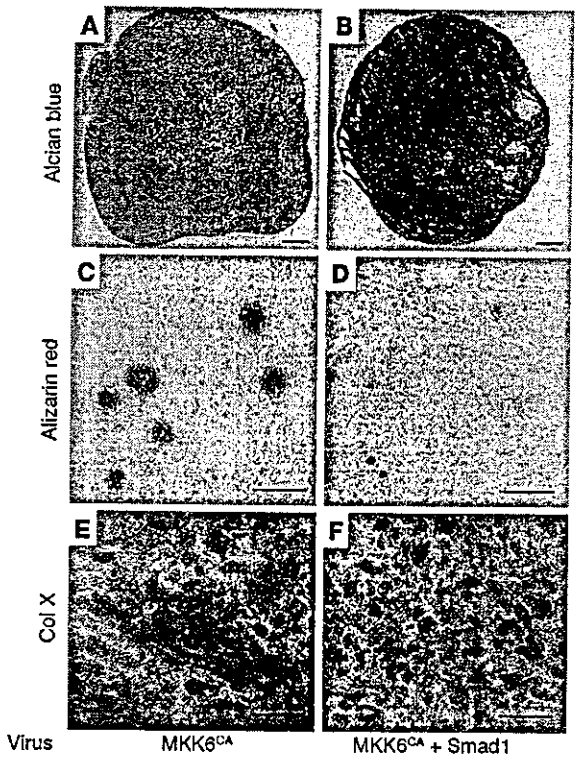

Figure 6
Induction of Alizarin red staining and type X collagen in MKK6-transduced SFs in pellet cultures. (A–F) SFs infected with MKK6^{CA} virus alone (A, C, and E) or together with Smad1 virus (B, D, and F) were subjected to pellet culture. Cultures were fixed with 3.7% formaldehyde 3 weeks later, and then stained with Alcian blue (A and B), Alizarin red (C and D) or anti–type X collagen (E and F). Note the increased Alcian blue staining and the reduced Alizarin red activity and type X collagen immunoactivity with Smad1 coexpression. Scale bars:100 μm (A–D) and 50 μm (E and F).

shown). The chondrogenic effect of ALK3^{CA} virus was further confirmed histologically by pellet cultures performed in vitro and in vivo (Figures 3 and 4). Induction of neither the osteoblast markers osteopontin and osteocalcin nor the terminal chondrocyte differentiation markers type X collagen and mineralization was observed in ALK3^{CA}-expressing cells (Figures 2, 3, 5, and 6). These results suggest that ALK3 signaling, that is, BMP signaling, has both stimulatory and regulatory roles in chondrogenesis: to induce the chondrogenic differentiation of SFs and at the same time to block their osteoblastic or hypertrophic differentiation. Despite the structural similarity between ALK3 and ALK6, the ALK6^{CA} virus was much less efficient in chondrogenesis, the reason for which remains to be clarified. Although many studies have demonstrated a prochondrogenic effect for TGF-β (15, 16, 20–22), we failed to find an anabolic effect for ALK5^{CA} which is expected to mimic TGF-β signaling, on the chondrogenic differentiation of SFs. We cannot fully explain the discrepancy between our results and those of previous studies, but Robbins and coworkers recently reported that adenovirus vector-mediated TGF-β gene transduction into arthritic joints in fact exacerbated cartilage degradation (38), raising the possibility that sustained activation of TGF-β signaling, via ALK5, has instead a negative effect on chondrogenesis. Further study will be required to elucidate the difference between TGF-β and BMP signaling.

The signaling of TGF-β/BMPs is transduced by Smad family members (31, 34, 35). Receptor-regulated Smads (R-Smads) are direct substrates of type I receptors and are phosphorylated at the C-terminal SSV/MS motif. R-Smads then form heteromeric complexes with common-mediator Smads and translocate into the nuclei, where they regulate transcription of target genes. In addition to Smad pathways, there is evidence that MAP kinase cascades are also implicated in ALK signaling, in which TGF-β–activating kinase (TAK1), a member of the MAP kinase kinase kinase family, plays a key role. TAK1 activates MAP kinase kinase in combination with an adaptor molecule, TAB1, which leads to JNK and p38 activation (32). The role of p38 in chondrogenesis has recently attracted particular interest because p38 inhibitors such as SB203580 suppress the chondrogenic differentiation of ATDC5 cells induced by growth/differentiation factor-5 (33, 39). However, the exact roles of the Smad pathways and p38 pathways in chondrocyte differentiation are not yet fully clarified. We used a combination of adenoviral gene delivery and a chemical inhibitor to segregate the roles of these two pathways downstream of ALK3 activation and found that (a) inhibitory Smad (Smad6) expression or treatment with the p38 inhibitor SB203580 suppressed the effect of ALK3^{CA} expression (Figure 2) (b) Smad1 synergistically augmented the effect of ALK3^{CA} (Figure 5A), and (c) activation of p38 pathways alone by MKK6^{CA} expression induced the hypertrophic differentiation markers type X collagen and mineralization in SFs, which was suppressed by Smad1 coexpression (Figures 5B and 6). These results suggest that although both Smad and p38 activation is necessary for chondrogenic differentiation of SFs, sustained activation of p38 pathways alone prompts the terminal differentiation of the cells. Consistent with our results, Zhen et al. (40) reported that parathyroid hormone inhibits type X collagen expression in hypertrophic chondrocytes by suppressing p38 pathways. Von der Mark et al. (41) reported the focal appearance of type X collagen in osteoarthritic cartilage, which may be involved in the degenerative changes of the articular cartilage and in the pathogenesis of osteoarthritis. Using the mouse model of osteoarthritis, we found that activated p38 is associated with type X colla-

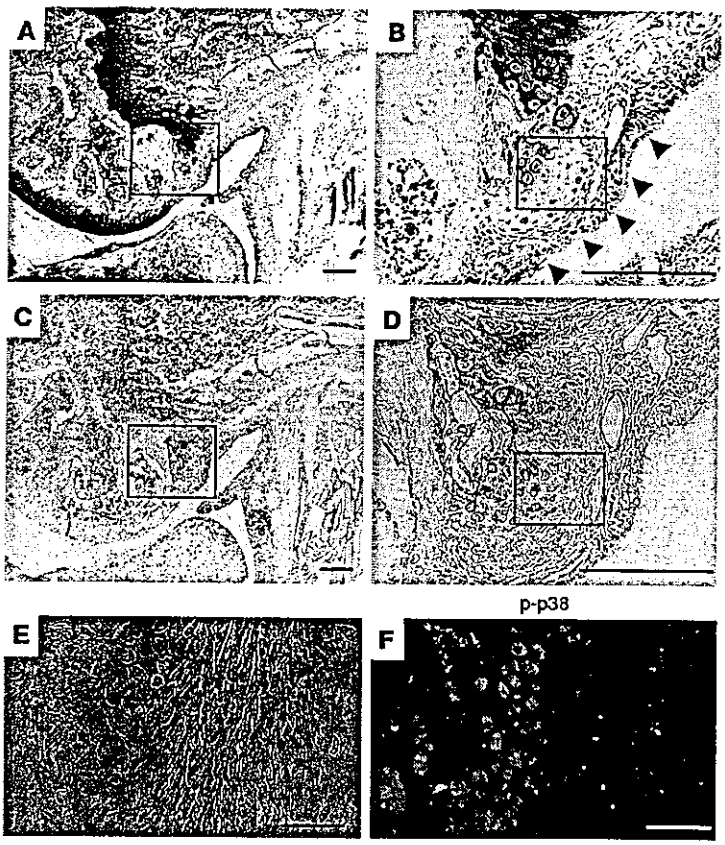

Figure 7
Histological analysis of knee joints in the mouse ACL and MM resection model. (**A–F**) Toluidine blue staining (**A** and **B**) and type X collagen immunostaining (**C** and **D**) at the marginal area between the articular cartilage and synovium. **B** and **D** present higher-magnification views of **A** and **C**, respectively. Osteochondrophytes were formed at the posterior edge of the femoral condyle, and they were positively stained by anti–type X collagen as well as toluidine blue (rectangular areas in **A** and **C**). Clusters of migrating synovial cells were observed adjacent to the osteochondrophytes (**B**, arrowheads) where future osteochondrophytes will develop, and they were positively stained by anti–type X collagen at the marginal area between synovium and osteophytes (rectangular area in **D**). This region was also positively stained by anti–phospho-p38 (**F**). **E** and **F** represent phase-contrast microscopy (**E**) and immunostaining with anti–phospho-p38 (**F**) of the rectangular area in **D**. Positive phospho-p38 staining was observed at the area of osteochondrophytes as well as the marginal synovium. Scale bars: 500 μm (**A–D**) and 50 μm (**E** and **F**).

gen expression in the synovial tissues adjacent to osteochondrophytes as well as in the degenerative cartilage (Figure 7).

Smad pathways not only are required for chondrogenic differentiation of SFs but also critically regulate the stage of differentiation of the cells and suppress their terminal differentiation process. Consistent with our findings, Scharstuhl recently reported inhibitory action of Smad7 in TGF-β–induced chondrocyte proliferation and proteoglycan production (42), indicating a critical role for Smad pathways. Hidaka and coworkers (43) demonstrated that adenovirus vector–mediated BMP-7 expression in chondrocytes accelerates the cartilage repair process. More recently, Lories and colleagues (44) demonstrated that BMP-2 and BMP-6 expressed in arthritic synovium are regulated by proinflammatory cytokines and differentially modulate fibroblast-like synoviocyte apoptosis, and Fukui et al. (45) found that BMP-2 expression was increased by proinflammatory cytokines in normal and osteoarthritis chondrocytes. These findings, combined with our observations, suggest that although BMPs have favorable effects on the repair process of articular cartilage, they may have proapoptotic and/or degenerative effects on the cells when p38 pathways are overactivated. Our findings suggest an important role for p38 signal transduction pathways in chondrocytes and SFs, leading to degenerative joint disorders, and suggest the potential utility of p38 modifiers in the treatment of rheumatoid arthritis and/or osteoarthritis. In fact, p38 kinase modifiers are now in clinical trials to treat rheumatoid arthritis (46). Based on our observations, we would like to propose that SFs are an excellent source for chondroprogenitors, which can be differentiated into chondrocytes via ALK3 activation, and that activation of the Smad pathway while controlling the degree of p38 activation may be a way to generate committed chondrocytes for the repair and/or replacement of cartilage.

Acknowledgments

The authors thank R. Yamaguchi and M. Ikeuchi (Department of Orthopaedic Surgery, The University of Tokyo), who provided expert technical assistance; K.L. Insogna (Yale University) for critical reading of the manuscript; and Y. Iwamoto (Thomas Jefferson University) for type II collagen and aggrecan probes. ALK and Smad adenovirus vectors were kindly provided by K. Miyazono (The University of Tokyo) and T. Imamura (The Cancer Institute of the Japanese Foundation for Cancer Research). This work was in part supported by Grants-in-Aid from the Ministry of Education, Culture, Sports, Science and Technology of Japan, Health Science research grants from the Ministry of Health and Welfare of Japan and an Uehara Memorial Award to S. Tanaka.

Received for publication August 28, 2003, and accepted in revised form January 6, 2004.

Address correspondence to: Sakae Tanaka, Department of Orthopaedic Surgery, Faculty of Medicine, The University of Tokyo, 7-3-1 Hongo, Bunkyo-ku, Tokyo 113-0033, Japan. Phone: 81-3-3815-5411 ext. 33376; Fax: 81-3-3818-4082; E-mail: TANAKAS-ORT@h.u-tokyo.ac.jp.

1. Hunziker, E.B. 2002. Articular cartilage repair: basic science and clinical progress. A review of the current status and prospects. *Osteoarthritis Cartilage.* 10:432–463.
2. Poole, A.R., et al. 2001. Composition and structure of articular cartilage: a template for tissue repair. *Clin. Orthop.* 391:S26–S33.
3. Poole, A.R. 2003. What type of cartilage repair are we attempting to attain? *J. Bone Joint Surg. Am.* 85-A(Suppl. 2):40–44.
4. Hunziker, E.B. 2003. Tissue engineering of bone and cartilage. From the preclinical model to the patient. *Novartis Found. Symp.* 249:70–85, 170–174, and 239–141.
5. Bruder, S.P., et al. 1998. Mesenchymal stem cells in osteobiology and applied bone regeneration. *Clin. Orthop.* 355:S247–S256.
6. Matsusue, Y., Yamamuro, T., and Hama, H. 1993. Arthroscopic multiple osteochondral transplantation to the chondral defect in the knee associated with anterior cruciate ligament disruption. *Arthroscopy.* 9:318–321.
7. Bentley, G., et al. 2003. A prospective, randomised comparison of autologous chondrocyte implantation versus mosaicplasty for osteochondral defects in the knee. *J. Bone Joint Surg. Br.* 85:223–230.
8. Peterson, L., Minas, T., Brittberg, M., and Lindahl, A. 2003. Treatment of osteochondritis dissecans of the knee with autologous chondrocyte transplantation: results at two to ten years. *J. Bone. Joint Surg. Am.* 85-A(Suppl 2):17–24.
9. Peterson, L., Brittberg, M., Kiviranta, I., Akerlund, E.L., and Lindahl, A. 2002. Autologous chondrocyte transplantation. Biomechanics and long-term durability. *Am. J. Sports Med.* 30:2–12.
10. Minas, T., and Nehrer, S. 1997. Current concepts in the treatment of articular cartilage defects. *Orthopedics.* 20:525–538.
11. Hangody, L., Feczko, P., Bartha, L., Bodo, G., and Kish, G. 2001. Mosaicplasty for the treatment of articular defects of the knee and ankle. *Clin. Orthop.* 391:S328–S336.
12. Firestein, G.S. 2003. Evolving concepts of rheumatoid arthritis. *Nature.* 423:356–361.
13. Takayanagi, H., et al. 1999. Suppression of arthritic bone destruction by adenovirus-mediated csk gene transfer to synoviocytes and osteoclasts. *J. Clin. Invest.* 104:137–146.
14. Hunziker, E.B., and Rosenberg, L.C. 1996. Repair of partial-thickness defects in articular cartilage: cell recruitment from the synovial membrane. *J. Bone Joint Surg. Am.* 78:721–733.
15. Nishimura, K., et al. 1999. Chondroprogenitor cells of synovial tissue. *Arthritis Rheum.* 42:2631–2637.
16. De Bari, C., Dell'Accio, F., Tylzanowski, P., and Luyten, F.P. 2001. Multipotent mesenchymal stem cells from adult human synovial membrane. *Arthritis Rheum.* 44:1928–1942.
17. De Bari, C., et al. 2003. Skeletal muscle repair by adult human mesenchymal stem cells from synovial membrane. *J. Cell Biol.* 160:909–918.
18. O'Connell, J.X. 2000. Pathology of the synovium. *Am. J. Clin. Pathol.* 114:773–784.
19. Wozney, J.M. 1989. Bone morphogenetic proteins. *Prog. Growth Factor Res.* 1:267–280.
20. Kulyk, W.M., Rodgers, B.J., Greer, K., and Kosher, R.A. 1989. Promotion of embryonic chick limb cartilage differentiation by transforming growth factor-beta. *Dev. Biol.* 135:424–430.
21. Lafeber, F.P., Vander Kraan, P.M., Van Roy, J.L., Huber-Bruning, O., and Bijlsma, J.W. 1993. Articular cartilage explant culture; an appropriate in vitro system to compare osteoarthritic and normal human cartilage. *Connect. Tissue Res.* 29:287–299.
22. Denker, A.E., Nicoll, S.B., and Tuan, R.S. 1995. Formation of cartilage-like spheroids by micromass cultures of murine C3H10T1/2 cells upon treatment with transforming growth factor-β 1. *Differentiation.* 59:25–34.
23. Yamamoto, A., et al. 2003. Suppression of arthritic bone destruction by adenovirus-mediated dominant-negative Ras gene transfer to synoviocytes and osteoclasts. *Arthritis Rheum.* 48:2682–2692.
24. Takayanagi, H., et al. 2000. Involvement of receptor activator of nuclear factor κB ligand/osteoclast differentiation factor in osteoclastogenesis from synoviocytes in rheumatoid arthritis. *Arthritis Rheum.* 43:259–269.
25. Tanaka, S., et al. 1998. Modulation of osteoclast function by adenovirus vector-induced epidermal growth factor receptor. *J. Bone Miner. Res.* 13:1714–1720.
26. Miyake, S., et al. 1996. Efficient generation of recombinant adenoviruses using adenovirus DNA-terminal protein complex and a cosmid bearing the full-length virus genome. *Proc. Natl. Acad. Sci. U. S. A.* 93:1320–1324.
27. Fujii, M., et al. 1999. Roles of bone morphogenetic protein type I receptors and Smad proteins in osteoblast and chondroblast differentiation. *Mol. Biol. Cell.* 10:3801–3813.
28. Enomoto-Iwamoto, M., et al. 2000. Hedgehog proteins stimulate chondrogenic cell differentiation and cartilage formation. *J. Bone Miner. Res.* 15:1659–1668.
29. Kamekura, S., et al. 2003. Establishment of novel experimental osteoarthritis models in mice. *J. Bone Miner. Res.* 18:S395.
30. van den Berg, W.B. 2001. Lessons from animal models of osteoarthritis. *Curr. Opin. Rheumatol.* 13:452–456.
31. Derynck, R., Zhang, Y., and Feng, X.H. 1998. Smads: transcriptional activators of TGF-β responses. *Cell.* 95:737–740.
32. Miyazono, K., Kusanagi, K., and Inoue, H. 2001. Divergence and convergence of TGF-β/BMP signaling. *J. Cell Physiol.* 187:265–276.
33. Watanabe, H., de Caestecker, M.P., and Yamada, Y. 2001. Transcriptional cross-talk between Smad, ERK1/2, and p38 mitogen-activated protein kinase pathways regulates transforming growth factor-β-induced aggrecan gene expression in chondrogenic ATDC5 cells. *J. Biol. Chem.* 276:14466–14473.
34. Miyazono, K. 1997. TGF-β receptors and signal transduction. *Int. J. Hematol.* 65:97–104.
35. Massague, J. 1998. TGF-β signal transduction. *Annu. Rev. Biochem.* 67:753–791.
36. de Crombrugghe, B., et al. 2000. Transcriptional mechanisms of chondrocyte differentiation. *Matrix Biol.* 19:389–394.
37. Akiyama, H., Chaboissier, M.C., Martin, J.F., Schedl, A., and de Crombrugghe, B. 2002. The transcription factor Sox9 has essential roles in successive steps of the chondrocyte differentiation pathway and is required for expression of Sox5 and Sox6. *Genes Dev.* 16:2813–2828.
38. Mi, Z., et al. 2003. Adverse effects of adenovirus-mediated gene transfer of human transforming growth factor beta 1 into rabbit knees. *Arthritis Res.* 5:R132–R139.
39. Nakamura, K., et al. 1999. p38 mitogen-activated protein kinase functionally contributes to chondrogenesis induced by growth/differentiation factor-5 in ATDC5 cells. *Exp. Cell Res.* 250:351–363.
40. Zhen, X., Wei, L., Wu, Q., Zhang, Y., and Chen, Q. 2001. Mitogen-activated protein kinase p38 mediates regulation of chondrocyte differentiation by parathyroid hormone. *J. Biol. Chem.* 276:4879–4885.
41. von der Mark, K., et al. 1995. Upregulation of type X collagen expression in osteoarthritic cartilage. *Acta Orthop. Scand. Suppl.* 266:125–129.
42. Scharstuhl, A., et al. 2003. Adenoviral overexpression of Smad-7 and Smad-6 differentially regulates TGF-β-mediated chondrocyte proliferation and proteoglycan synthesis. *Osteoarthritis Cartilage.* 11:773–782.
43. Hidaka, C., et al. 2003. Acceleration of cartilage repair by genetically modified chondrocytes over expressing bone morphogenetic protein-7. *J. Orthop. Res.* 21:573–583.
44. Lories, R.J., Derese, I., Ceuppens, J.L., and Luyten, F.P. 2003. Bone morphogenetic proteins 2 and 6, expressed in arthritic synovium, are regulated by proinflammatory cytokines and differentially modulate fibroblast-like synoviocyte apoptosis. *Arthritis Rheum.* 48:2807–2818.
45. Fukui, N., Zhu, Y., Maloney, W.J., Clohisy, J., and Sandell, L.J. 2003. Stimulation of BMP-2 expression by pro-inflammatory cytokines IL-1 and TNF-α in normal and osteoarthritic chondrocytes. *J. Bone Joint Surg. Am.* 85-A(Suppl. 3):59–66.
46. Pargellis, C., and Regan, J. 2003. Inhibitors of p38 mitogen-activated protein kinase for the treatment of rheumatoid arthritis. *Curr. Opin. Investig. Drugs.* 4:566–571.

Research article Related Commentary, page 805

PPARγ insufficiency enhances osteogenesis through osteoblast formation from bone marrow progenitors

Toru Akune,[1] Shinsuke Ohba,[2] Satoru Kamekura,[1] Masayuki Yamaguchi,[1] Ung-il Chung,[2] Naoto Kubota,[3] Yasuo Terauchi,[3] Yoshifumi Harada,[4] Yoshiaki Azuma,[4] Kozo Nakamura,[1] Takashi Kadowaki,[3] and Hiroshi Kawaguchi[1]

[1]Department of Orthopaedic Surgery, [2]Department of Tissue Engineering, and [3] Department of Metabolic Diseases, Faculty of Medicine, University of Tokyo, Tokyo, Japan. [4]Teijin Co., Tokyo, Japan.

Based on the fact that aging is associated with a reciprocal decrease of osteogenesis and an increase of adipogenesis in bone marrow and that osteoblasts and adipocytes share a common progenitor, this study investigated the role of PPARγ, a key regulator of adipocyte differentiation, in bone metabolism. Homozygous *PPARγ*-deficient ES cells failed to differentiate into adipocytes, but spontaneously differentiated into osteoblasts, and these were restored by reintroduction of the *PPARγ* gene. Heterozygous *PPARγ*-deficient mice exhibited high bone mass with increased osteoblastogenesis, but normal osteoblast and osteoclast functions, and this effect was not mediated by insulin or leptin. The osteogenic effect of PPARγ haploinsufficiency became prominent with aging but was not changed upon ovariectomy. The PPARγ haploinsufficiency was confirmed to enhance osteoblastogenesis in the bone marrow cell culture but did not affect the cultures of differentiated osteoblasts or osteoclast-lineage cells. This study demonstrates a PPARγ-dependent regulation of bone metabolism in vivo, in that PPARγ insufficiency increases bone mass by stimulating osteoblastogenesis from bone marrow progenitors.

Introduction

Osteoblasts and adipocytes share a common progenitor: multipotential mesenchymal stem cells in bone marrow (1–3). Accumulated evidence of the differentiation switching of these two cell lineages suggests that a large degree of plasticity exists between them and that the relationship is reciprocal (4–6). The clinical fact that a decrease in bone volume (BV) of age-related osteoporosis is accompanied by an increase in marrow adipose tissue (7–9) also implies the possible reciprocal relationship that is postulated to exist between the two differentiation pathways. The signal transduction pathways implicated in this process are therefore evaluated as potential targets for therapeutic intervention of osteoporosis. The molecular mechanism underlying the reciprocal relationship is not yet well understood, however, although several studies using strain-specific and KO murine models have begun to explore the relationship in vivo (10–15).

Several key transcription factors that function in the complex transcriptional cascade during adipocyte differentiation have been identified, including PPARγ and CCAAT enhancer-binding proteins (C/EBPs) (16). PPARγ is a ligand-activated transcription factor that belongs to the nuclear hormone receptor superfamily and functions as a heterodimer with a retinoid X receptor by binding to the PPAR responsive element (PPRE) within the promoters of the target genes (17–19). PPARγ is expressed early in the adipocyte differentiation program and is activated by long-chain fatty acids, peroxisome proliferators, and the thiazolidinedione class of antidiabetic agents (17–19). Most importantly, PPARγ plays requisite and sufficient roles in the regulation of adipocyte differentiation, because its overexpression in fibroblast cell lines initiates adipogenesis (20) and ES cells and embryonic fibroblastic cells from mice lacking *PPARγ* were unable to differentiate into adipocytes (21–23).

When one takes the results of the studies together, it is possible that PPARγ may contribute not only to adipogenesis, but also to osteogenesis in the bone marrow where bipotential precursors can differentiate to either adipocytes or osteoblasts. This study investigated the physiological role of PPARγ on the marrow cells and bone cells using in vivo morphological analyses and ex vivo cell culture systems. For the in vivo analysis, we used mice lacking the *PPARγ* gene, which we generated by gene targeting (22). Although the homozygous *PPARγ*-deficient (*PPARγ*$^{-/-}$) mice were embryonically lethal at 10.5–11.5 days after post coitum due to placental dysfunction, heterozygous *PPARγ*-deficient (*PPARγ*$^{+/-}$) mice developed normally. The heterozygotes led to a 50% reduction in PPARγ expression and exhibited resistance to high-fat diet–induced obesity and insulin resistance; however, on a standard diet they grew normally, without abnormalities in major organs such as brain, heart, liver, spleen, or kidney (22, 24). We show here that the homozygous *PPARγ*-deficient ES cells spontaneously differentiate into osteoblasts ex vivo and that PPARγ haploinsufficiency due to the heterozygous *PPARγ* deficiency resulted in enhanced bone formation with increased osteoblastogenesis from bone marrow progenitors both in vivo and ex vivo.

Methods

Animals. The generation of *PPARγ* gene-targeted mice was described previously (22). In each experiment, WT and *PPARγ*$^{+/-}$

Nonstandard abbreviations used: alkaline phosphatase (ALP); bone morphogenetic protein-2 (BMP-2); bone volume (BV); CCAAT enhancer-binding proteins (C/EBPs); computed tomography (CT); LDL receptor–related protein 5 (LRP5); leukemia inhibitory factor (LIF); M-CSF–dependent bone marrow macrophage (M-BMMϕ); receptor activator of nuclear factor κB ligand (RANKL); ovariectomy (OVX); PPAR responsive element (PPRE); tartrate-resistant acid phosphatase (TRAP); tissue volume (TV); type I collagen α1 chain (COL1A1).

Conflict of interest: The authors have declared that no conflict of interest exists.

Citation for this article: *J. Clin. Invest.* 113:846–855 (2004). doi:10.1172/JCI200419900.

mice littermates fed a standard diet were compared. All experiments were performed on male mice at 8 or 52 weeks of age, except for the ovariectomy (OVX) experiment in which female mice underwent surgical operation at 26 weeks and were analyzed at 30 weeks. All experiments were performed according to the protocol approved by the Animal Care and Use Committee of the University of Tokyo.

ES cell cultures. Mouse *PPARγ*$^{-/-}$ and WT ES cells were isolated from blastocysts generated by mating *PPARγ*$^{+/-}$ mice with each other, as previously described (25). ES cells were maintained in DMEM medium supplemented with 15% FBS, 200 mM L-glutamine, 100 μM β-mercaptoethanol, and 10^3 U/ml of leukemia inhibitory factor (LIF; Chemicon International, Temecula, California, USA). Differentiation of ES cells was induced by using a modified protocol, described previously (2, 26). In brief, after being trypsinized with 0.025% trypsin-EDTA, cells were plated onto a bacterial Petri dish in the absence of LIF and cultured with 100 nM all-*trans* retinoic acid for 5 days, with medium being replenished on day 3. The embryoid bodies were transferred to a gelatinized six-multiwell plate and allowed to adhere to the well with DMEM containing 10% FBS. For the analysis of osteogenic differentiation, cultures were maintained in the same condition without any additional supplements for 10 days, were fixed with 10% buffered formalin, and were incubated in the presence of 5% silver nitrate solution under an ultraviolet light for 10 minutes, then incubated for 5 minutes in the presence of 5% sodium thiosulfate solution (von Kossa staining). To discern the calcified nodules from the embryoid body, both of which are seen as black, the von Kossa–positive nodules that do not connect to the embryoid body in a well were counted. For the analysis of adipogenesis, the medium was supplemented with 1 μM troglitazone (Sankyo Pharmaceutical Co., Tokyo, Japan) for 10 days, fixed in 10 mM sodium periodate, 2% paraformaldehyde, 75 mM L-lysin dihydrochloride, and 37.5 mM sodium phosphate, and then stained in a filtered solution of 0.3% oil red O in 60% isopropanol for 15 minutes. The red-stained, lipid vacuole–containing cells in a well were counted. To rescue osteoblast and adipocyte differentiation of *PPARγ*$^{-/-}$ ES cells, the recombinant retrovirus vector carrying the *PPARγ* gene and empty vector were constructed as previously described (22). ES cells were infected with equal titers of each recombinant virus as described (20), with some modification.

Skeletal morphology and blood chemistry. A bone radiograph was taken with a soft x-ray apparatus (SOFTEX; CMB-2, Tokyo, Japan). A three-dimensional CT scan was taken using a composite x-ray analyzing system (NX-HCP; NS-ELEX Inc., Tokyo, Japan) and the trabecular bone area (percentage of BV per tissue volume [TV]) was measured on the computed tomography (CT) image. All histological analyses were carried out using WT and *PPARγ*$^{-/-}$ littermates as previously described (27). Parameters for the trabecular bone and the number of bone marrow adipocytes was measured in an area 1.2 mm in length from 0.5 mm below the growth plate at the proximal metaphysis of the tibiae. The number of adipocytes in this area was determined by counting that of oval vacuoles in the toluidine blue staining. The thickness of the growth plate was measured at the proximal tibiae. Serum insulin was measured by insulin immunoassay (Morinaga Institute of Biological Science, Yokohama, Japan), and leptin was assayed with the ELISA-based Quantikine M mouse leptin immunoassay kit (R&D Systems Inc., Minneapolis, Minnesota, USA).

Primary bone marrow cell cultures. Bone marrow cells were collected from long bones of 8-week-old *PPARγ*$^{-/-}$ and WT male littermates. Cells were plated at a density of 10^6 cells on a six-multiwell plate in α-MEM containing 10% FBS, with 1 μM troglitazone for the adipogenesis assay and with 50 μg/ml ascorbic acid and 10 mM β-glycerophosphate for osteogenesis assay. The oil red O staining was performed as mentioned above at 14 days of culture. For the alkaline phosphatase (ALP), cultured plates were rinsed with PBS, fixed in 100% ethanol at 10 days of culture, and stained with Tris-HCl–buffered solution (pH 9.0) containing naphthol AS-MX phosphate as a substrate and Fast Blue BB salt (Sigma-Aldrich, St. Louis, Missouri, USA) as a coupler. For the Alizarin red S staining, cultured plates were rinsed with PBS at 21 days of culture, fixed in 10% buffered formalin, and stained with 2% Alizarin red S (pH 4.0) (Sigma-Aldrich). The von Kossa staining was performed as mentioned above at 28 days of culture. For the growth curve assay, bone marrow cells derived from either WT or *PPARγ*$^{+/-}$ littermates were inoculated at a density of 10^7 cells per dish in 10-cm culture dishes in α-MEM containing 10% FBS, 50 μg/ml ascorbic acid, and 10 mM β-glycerophosphate, and then was cultured for 3 days. The adherent cells were then harvested and inoculated at a density of 3×10^5 cells/dish in 10-cm culture dishes and further cultured in the same medium. The number of cells per dish was counted 1, 2, 3, and 4 days after the seeding.

Real-time quantitative RT-PCR. Total RNA was extracted with an ISOGEN kit (Wako Pure Chemicals Industry Ltd., Osaka, Japan), according to the manufacturer's instructions, from ES cells cultured for 10 days after the embryoid bodies were transferred to gelatinized plates and from bone marrow cells cultured for 14 days after the seeding. One microgram of RNA was reverse-transcribed using a Takara RNA PCR Kit (AMV) ver. 2.1 (Takara Shuzo Co., Shiga, Japan) to make single-stranded cDNA. PCR was performed on an ABI Prism 7000 Sequence Detection System (Applied Biosystems Inc., Foster City, California, USA). The PCR reactions consisted of QuantiTect SYBR Green PCR Master Mix (QIAGEN, Tokyo, Japan), 0.3 μM specific primers, and 500 ng of cDNA. Relative levels of mRNA of a specific gene were calculated using the standard curve generated with cDNA dilutions, with normalization to actin as an internal control. PCR primers of specific genes used for amplification are available upon request.

Primary osteoblastic cell cultures. Osteoblastic cells were isolated from calvariae of neonatal WT and *PPARγ*$^{-/-}$ littermates as previously described (27). For the cell proliferation assay, cells were inoculated at a density of 10^4 cells/well in a 24-multiwell plate, cultured in the same medium for 48 hours, and deprived of serum for 12 hours before adding the experimental medium with and without troglitazone (1 μM) or FGF-2 (1 nM; Kaken Pharmaceutical Co., Chiba, Japan). Incorporation of [^{3}H]-thymidine (1 μCi/ml in the medium) added for the final 3 hours was measured after 24 hours of culture. For ALP activity measurement, cells were inoculated at a density of 10^4 cells/well in a 24-multiwell plate and cultured in α-MEM containing 10% FBS and 50 μg/ml ascorbic acid with and without troglitazone (1 μM) or bone morphogenetic protein-2 (BMP-2; 30 ng/ml; Yamanouchi Pharmaceutical Co., Tokyo, Japan). At 14 days of culture, cells were sonicated in 10 mM Tris-HCl buffer (pH 8.0) containing 1 mM $MgCl_2$ and 0.5% Triton X-100. ALP activity in the lysate was measured using a Wako ALP kit (Wako Pure Chemicals Industry Ltd.), and the protein content was determined using a BCA protein assay reagent (Pierce Chemical Co., Rockford, Illinois, USA). For Alizarin red S and von Kossa stainings, cells were inoculated at a density of 5×10^4 cells/well in a six-multiwell plate in α-MEM containing 10% FBS, 50 μg/ml ascorbic acid, and 10 mM β-glyc-

erophosphate, and were stained at day 21 and 28, respectively, as mentioned above. Difference in maturity between the bone marrow cells and the calvarial osteoblasts was examined by the calcified nodule formation determined by Alizarin red S staining and the osteocalcin expression determined by real-time PCR analysis.

Assays for osteoclastic cells. Tartrate-resistant acid phosphatase-positive (TRAP-positive) multinucleated osteoclasts were generated by coculturing osteoblastic cells (10^4 cells/well) and bone marrow cells (5×10^5 cells/well) derived from either WT or *PPARγ*$^{-/-}$ littermates, as mentioned above, in a 24-multiwell plate in α-MEM containing 10% FBS for 6 days with and without $1,25(OH)_2D_3$ (10 nM), prostaglandin E_2 (100 nM), and IL-11 (10 ng/ml). Cells positively stained for TRAP containing more than three nuclei were counted as osteoclasts. To determine bone resorption activity, osteoclasts formed by the coculture on 0.24% collagen gel coated on 100-mm dishes were digested with 0.2% collagenase solution, and a 1:50 aliquot including osteoclasts was seeded on a dentine slice. After 48 hours of culture in α-MEM containing 10% FBS, the total area of pits stained with 0.5% toluidine blue was evaluated using an image analyzer. To study the role of PPARγ intrinsic to osteoclastic cells, we used the M-CSF–dependent bone marrow macrophage (M-BMMϕ) culture system as described previously (28). Briefly, bone marrow cells from WT or *PPARγ*$^{-/-}$ mice were seeded at a density of 3×10^5 cells/well in a 24-multiwell plate and cultured in α-MEM containing 10% FBS with M-CSF (100 ng/ml). After culturing for 3 days, adherent cells (M-BMMϕ) were further cultured with M-CSF (100 ng/ml) and soluble receptor activator of nuclear factor κB ligand (RANKL) (100 ng/ml) for 3 days. TRAP-positive osteoclasts were counted. To determine the survival, osteoclasts generated as above were deprived of M-CSF/soluble RANKL and cultured for an additional 48 hours. At 3, 6, 12, 24, and 48 hours, the TRAP-positive and trypan blue–negative osteoclasts were counted.

Statistical analysis. Means of groups were compared by ANOVA, and significance of differences was determined by post-hoc testing using Bonferroni's method.

Results

Osteogenesis is enhanced in the homozygous PPARγ-deficient ES cell culture. To examine the involvement of the PPARγ signaling in fat and bone metabolism, we first compared the adipogenesis and osteogenesis in

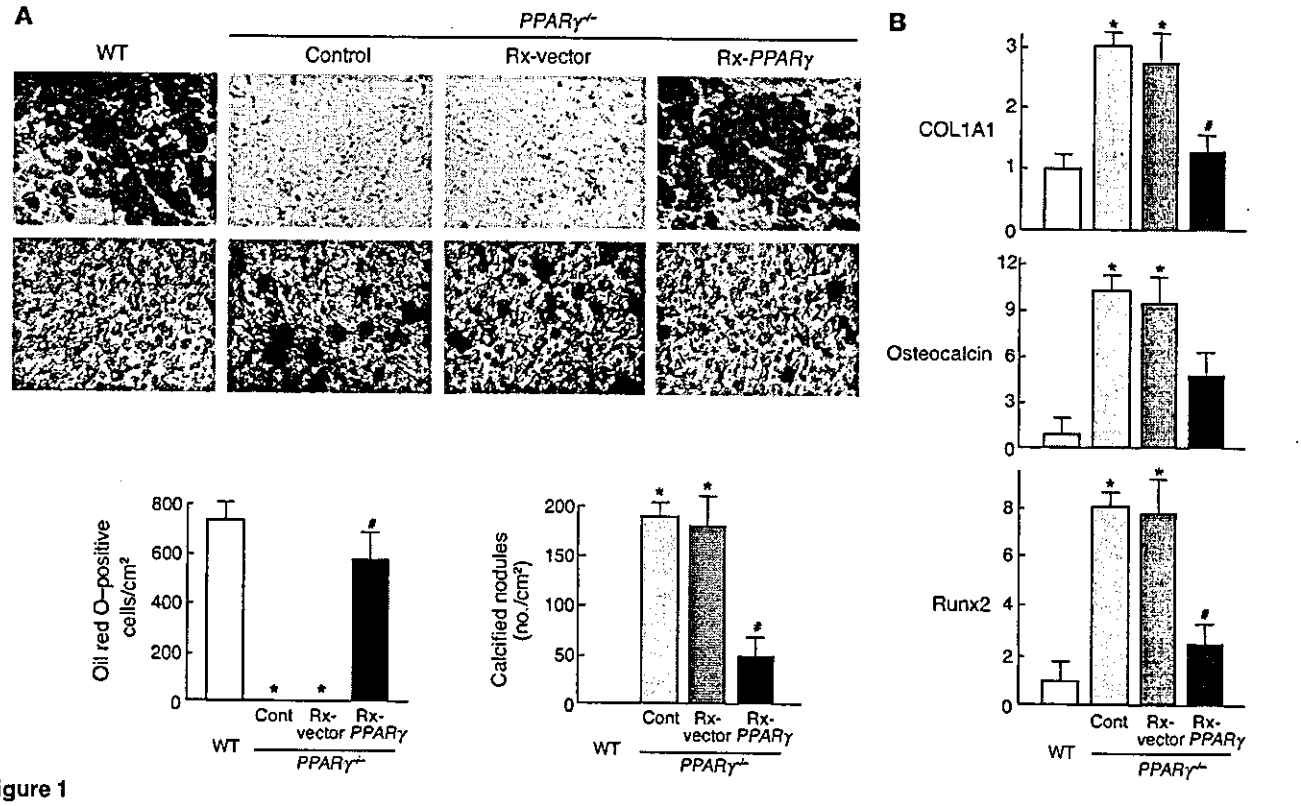

Figure 1

Adipogenesis and osteogenesis in the mouse ES cell cultures of homozygous *PPARγ*-deficient (*PPARγ*$^{-/-}$) and WT genotypes. As a rescue experiment, PPARγ was reintroduced into *PPARγ*$^{-/-}$ ES cells using a retrovirus vector carrying the *PPARγ* gene (Rx-*PPARγ*) or the same retrovirus vector without the *PPARγ* gene (Rx-vector) as a control. (**A**) The upper row shows the adipogenesis determined by the oil red O staining of the ES cell culture in DMEM/10% FBS with troglitazone. The number of oil red O–positive cells stained in red was counted and shown in the left graph as the cells per square centimeter. The images in the lower row indicate the osteogenesis determined by the von Kossa staining of the ES cell culture in DMEM/10% FBS without any osteogenic supplements. The number of von Kossa–positive calcified nodules stained in black was counted and shown in the right graph as the number per square centimeter. Scale bar: 20 μm. (**B**) Relative mRNA levels of the marker genes for osteoblasts — COL1A1, osteocalcin and Runx2 — determined by real-time quantitative RT-PCR 10 days after the embryoid bodies were transferred to a gelatinized six-multiwell plate in DMEM/10% FBS without any osteogenic supplements. The ordinate axis indicates the relative amount of mRNA as compared with that of WT. Data are expressed as means (bars) ± SEMs (error bars) for eight wells per group. *Significant difference from the WT culture, $P < 0.01$. #Significant restoration by Rx-*PPARγ* as compared with the control *PPARγ*$^{-/-}$ and *PPARγ*$^{-/-}$ plus Rx-vector cultures; $P < 0.01$. Cont, control.